



**METEOROLOGICAL
SERVICE
SINGAPORE**
Centre for Climate Research Singapore

Appendix to Chapter 3

Sub-selection of CMIP5 GCMs for downscaling over Singapore

Authors: Carol McSweeney¹, Raizan Rahmat², Grace Redmond¹, Charline Marzin², James Murphy¹, Richard Jones¹, Wee-Kiong Cheong², See-Yee Lim² and Xiangming Sun²

1 - Met Office, Exeter, UK

2 - Centre for Climate Research Singapore, Singapore

© COPYRIGHT RESERVED 2015

All rights reserved. No part of this publication may be reproduced, stored in a retrievable system, or transmitted in any form or by any means, electronic or mechanical, without prior permission of the Government of Singapore.

Contents

Appendix 3.1: Contextual information: CMIP3 and CMIP5 projections for Southeast Asia	2
Appendix 3.2: Details of CMIP5 GCMs analysed.....	5
Models with 6hrly variables available for use in RCM experiments are highlighted in grey.	5
* The FGOALS-S2 models have been withdrawn from the CMIP5 archive.....	6
Appendix 3.3: Validation Results	6
A3.3.1 Monsoon Circulations	6
A3.3.1.1 South West (SW) Monsoon.....	6
A3.1.2 North East (NE) Monsoon	11
3.3.2 Seasonal rainfall patterns.....	14
3.3.2.1 ITCZ migration.....	14
3.3.2.2 Annual rainfall cycles.....	17
3.3.3 Sea surface and air temperatures	19
3.4 Key Modes of Variability	25
3.4.1 ENSO and tele-connections in Southeast Asia	25
3.4.2 Madden-Julian Oscillation (MJO).....	26
Appendix 3.4: Tropical Cyclone (TC) assessment methodology	28
3.4.1 Tracking Methodology.....	28
3.4.2 Results.....	29
3.4.3 Comments on method and results	30
Appendix 3.5: Description of sub-regions used to characterise the annual rainfall cycle.....	35
References.....	36

Appendix 3.1: Contextual information: CMIP3 and CMIP5 projections for Southeast Asia

The availability of the new CMIP5 projections and the imminent IPCC fifth assessment report (AR5) will inevitably prompt those with an interest in using information about possible future climate to ask whether there are any substantial changes to the projections from CMIP5 compared to the preceding CMIP3 ensemble.

Due to a number of differences in the way that CMIP5 has been undertaken compared with CMIP3 means that direct comparisons between CMIP3 and CMIP5 are not possible. Firstly, the CMIP5 simulations have been driven using the new representative concentration pathways (RCPs) rather than the SRES emissions scenarios used previously (Moss et al., 2010). While the A1B emissions scenario is broadly equivalent with the RCP6.0, in terms of the forcing exerted by 2100, the remaining scenarios are not similarly equivalent. Secondly, assessing the 'range' across the ensemble for a comparable scenario is restricted by the differences in priorities ascribed to each scenario. In CMIP3, the largest number of available projections was generated under the 'mid-range' A1B scenario within the SRES family of non-mitigation emissions pathways. In CMIP5, RCPs 4.5 and 8.5 were identified as 'tier 1' priority experiments, such that the archive is less well populated for the 'tier 2' RCP2.6 and 6.0 experiments. However, while a comparison may not be direct, an investigation into the differences between the projections will provide an overview of whether the *key messages* regarding uncertainty and the nature of the future projections of future climate have changed substantially as a result of progress in modelling since CMIP3. Global assessments have indicated that there has been remarkably little change in the messages from CMIP5 projections in comparison to CMIP3 regarding the degree of agreement between models in the ensemble as a result of progress in modelling since CMIP3 (Knutti and Sedlacek, 2012;McSweeney and Jones, 2013).

We show in figures A3.1-A3.3 some comparisons between CMIP3 and CMIP5 projections for 2 regions – a wider Southeast Asia region as well as the Malaysian Peninsula. Figures A3.1 shows comparisons between the area-mean seasonal changes in temperature and precipitation in the CMIP3 SRESA1B and CMIP5 RCP6.0 simulations. The A1B and RCP6.0 scenarios are approximately equivalent in terms of total radiative forcing but RCP6.0 includes projections from fewer CMIP5 models than other RCPs. CMIP5 results from the RCP 4.5, 6.0 and 8.5 scenarios are compared in Figure A3.2 (RCP2.6 is omitted because this scenario differs substantially from the SRES scenarios).

The range of projections of average precipitation change under CMIP5 RCP6.0 over the wider SEA region is wider than CMIP3 SRESA1B, particularly in DJF and MAM, due mainly to one or two outliers (notably, a single CMIP5 model indicates significantly drier projections than any CMIP3 members). In summary, the majority of models in both ensembles indicate increases in mean rainfall in most seasons over the wider south-east Asia region, although a minority of CMIP5 models indicate drying. For the Malaysian Peninsula, we see that both ensembles span both increases and decreases in precipitation, but with a shift in CMIP5 towards a larger number of drying models in JJA and SON. The shift towards drying for the Malaysian Peninsula seems to partially reflect the limited sampling of CMIP5 models available for this scenario based on inconsistencies with the RCPs 4.5 and 8.5 results in Figure A3.2.

Similarly, a reduction in the range of temperature changes in CMIP5 compared with CMIP3 largely reflects the absence of a single outlier, affecting projections for the wider SEA region as well as the Malaysian Peninsula specifically.

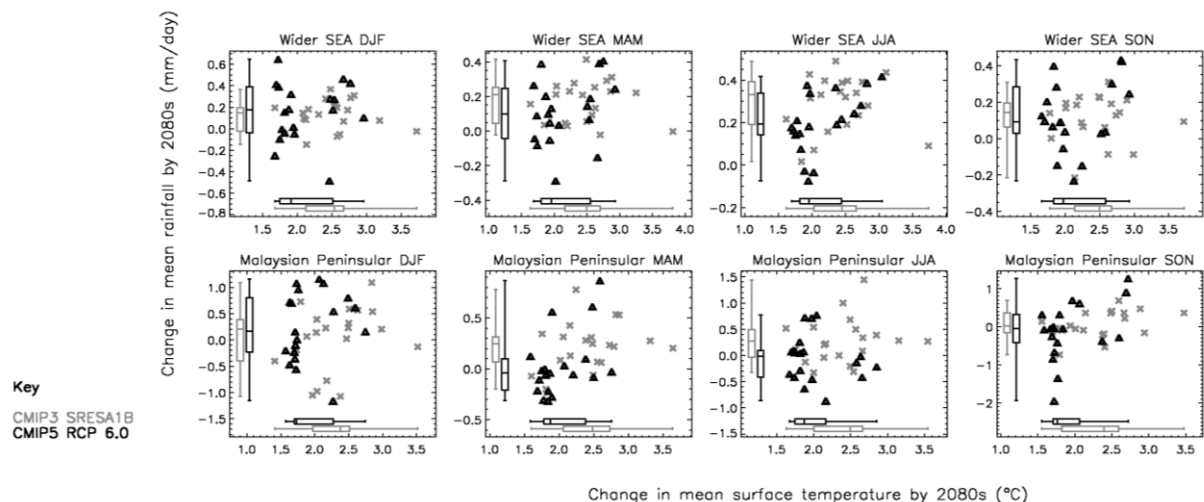


Figure A3.1: Scatter plots show the areal-average change in temperature and precipitation for two regions: the wider Southeast Asia region (80-150E, 30S-30N) and the Malaysian Peninsula (85-115E, 8.5S-10N) from the CMIP3 (SRESA1B) and CMIP5 (RCP6.0) ensemble projections. Boxplots indicate the median and inter-quartile range of each ensemble and the whiskers indicate the full range. Values indicate differences between 2070-2100 projection from 1961-90 baseline.

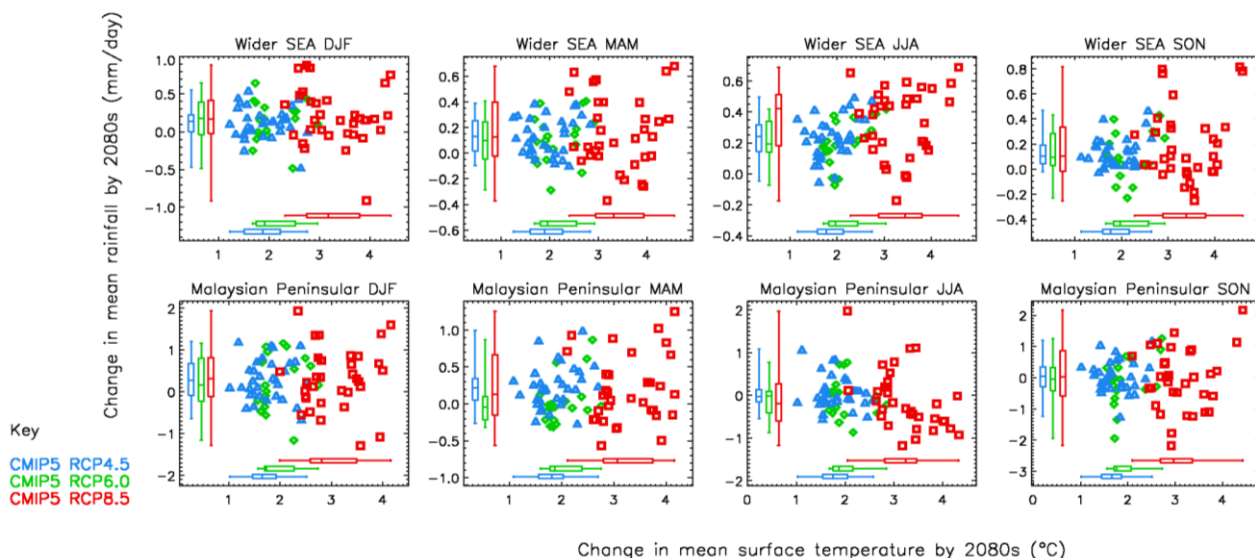


Figure A3.2: Scatter plots show the areal-average change in temperature and precipitation for two regions: the wider Southeast Asia region (80-150E, 30S-30N) and the Malaysian Peninsula (85-107E, 8.5S-10N) from the CMIP5 under 3 RCP scenarios. Boxplots indicate the median and inter-quartile range of each ensemble and the whiskers indicate the full range. Values indicate differences between 2070-2100 projection from 1961-90 baseline.

Some important differences in the messages for users regarding the ‘uncertainty’ indicated by the level of agreement in CMIP3 and CMIP5 multi-models ensembles (particularly with respect to rainfall) reflect progress in understanding the most appropriate way to measure ensemble agreement. Recent papers by Tebaldi, 2011; Knutti and Sedlacek, 2012 and McSweeney and Jones (2013) have considered methods by which model agreement is measured and displayed, highlighting the importance of considering whether projected changes are statistically significant. Identifying where projected changes in rainfall are statistically significant provides key differentiation between situations where projections span zero because all model project changes close to zero, and where there is a substantial ensemble disagreement in the direction of the change in rainfall. Figure A3.3 shows an ensemble consistency plot, based on the methodology described in McSweeney and Jones (2013), which includes this information about statistical significance. This method of diagnosing consistency shows that on the whole, we do not see much change in the degree of consistency in projections between the CMIP3 A1B and CMIP5 RCP6.0 projections for Southeast Asia in DJF – generally most models indicate that changes in rainfall are within the range of natural variability in both ensembles. However, for JJA, there does seem to be some shift away from the projections of rainfall increases that are shown for north of the Equator in CMIP3 A1B, towards a majority projection of ‘no significant change’ in average rainfall.

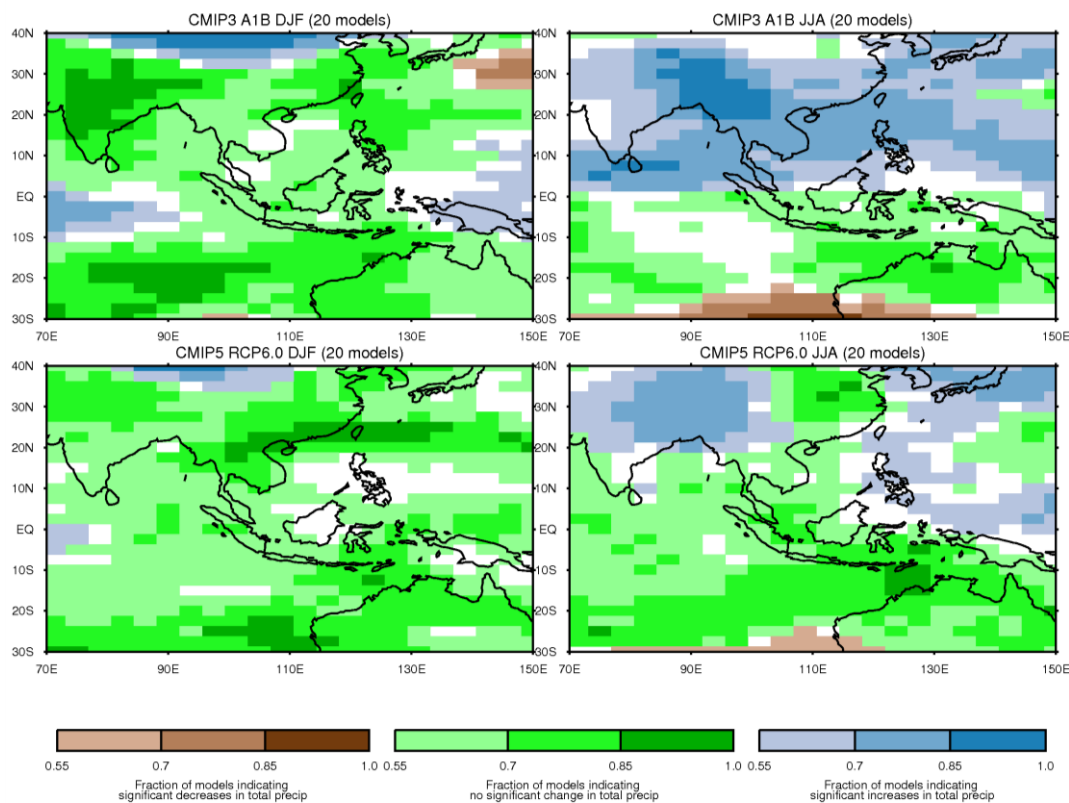


Figure A3.3: Comparison between the consistency in projections of future rainfall for the CMIP3 and CMIP5 ensembles. CMIP3 and CMIP5 projections are shown for the SRES A1B and RCP6.0 scenarios respectively. The colour used indicates the majority outcome between three alternatives of “statistically significant increases”, ‘statistically significant decreases’ or ‘change is not statistically significant’ (white indicates no majority), after McSweeney and Jones, (2013).

Appendix 3.2: Details of CMIP5 GCMs analysed

Models with 6hrly variables available for use in RCM experiments are highlighted in grey.

Modelling Group	Group Acronym	Model Designation
Commonwealth Scientific and Industrial Research Organization (CSIRO) and Bureau of Meteorology (BOM), Australia	CSIRO-BOM	ACCESS1-0
Commonwealth Scientific and Industrial Research Organization (CSIRO) and Bureau of Meteorology (BOM), Australia	CSIRO-BOM	ACCESS1-3
Beijing Climate Center, China Meteorological Administration	BCC	bcc-csm1-1
Beijing Climate Center, China Meteorological Administration	BCC	bcc-csm1-1-m
College of Global Change and Earth System Science, Beijing Normal University	GCESS	BNU-ESM
Canadian Centre for Climate Modelling and Analysis	CCCMA	CanESM2
National Center for Atmospheric Research	NCAR	CCSM4
Community Earth System Model Contributors	NSF-DOE-NCAR	CESM1-CAM5
Community Earth System Model Contributors	NSF-DOE-NCAR	CESM1-WACCM
Centro Euro-Mediterraneo per I Cambiamenti Climatici	CMCC	CMCC-CESM
Centro Euro-Mediterraneo per I Cambiamenti Climatici	CMCC	CMCC-CM
Centro Euro-Mediterraneo per I Cambiamenti Climatici	CMCC	CMCC-CMS
Centre National de Recherches Météorologiques / Centre Européen de Recherche et Formation Avancée en Calcul Scientifique	CNRM-CERFACS	CNRM-CM5
Commonwealth Scientific and Industrial Research Organization in collaboration with Queensland Climate Change Centre of Excellence	CSIRO-QCCCE	CSIRO-Mk3-6-0
EC-EARTH consortium	ICHEM	EC-EARTH
LASG, Institute of Atmospheric Physics, Chinese Academy of Sciences and CESS, Tsinghua University	LASG-CESS	FGOALS-g2
LASG, Institute of Atmospheric Physics, Chinese Academy of Sciences and CESS, Tsinghua University	LASG-IAP	FGOALS-s2*
The First Institute of Oceanography, SOA, China	FIO	FIO-ESM
NOAA Geophysical Fluid Dynamics Laboratory	NOAA GFDL	GFDL-CM3
NOAA Geophysical Fluid Dynamics Laboratory	NOAA GFDL	GFDL-ESM2G
NOAA Geophysical Fluid Dynamics Laboratory	NOAA GFDL	GFDL-ESM2M
NASA Goddard Institute for Space Studies	NASA-GISS	GISS-E2-H
NASA Goddard Institute for Space Studies	NASA-GISS	GISS-E2-H-CC
NASA Goddard Institute for Space Studies	NASA-GISS	GISS-E2-R
NASA Goddard Institute for Space Studies	NASA-GISS	GISS-E2-R-CC
Met Office Hadley Centre	MOHC	HadCM3
Met Office Hadley Centre	MOHC	HadGEM2-CC
Met Office Hadley Centre	MOHC	HadGEM2-ES
National Institute of Meteorological Research/Korea Meteorological Administration	NIMR/KMA	HadGEM2-A0
Institute for Numerical Mathematics	INM	inmcm4
Institut Pierre-Simon Laplace	IPSL	IPSL-CM5A-LR
Institut Pierre-Simon Laplace	IPSL	IPSL-CM5A-MR
Institut Pierre-Simon Laplace	IPSL	IPSL-CM5B-LR
Japan Agency for Marine-Earth Science and Technology, Atmosphere and Ocean Research Institute (The University of Tokyo), and National Institute for Environmental Studies	MIROC	MIROC-4h
Japan Agency for Marine-Earth Science and Technology, Atmosphere and Ocean Research Institute (The University of Tokyo), and National Institute for Environmental Studies	MIROC	MIROC5
Japan Agency for Marine-Earth Science and Technology, Atmosphere and Ocean Research Institute (The University of Tokyo), and National Institute for Environmental Studies	MIROC	MIROC-ESM
Japan Agency for Marine-Earth Science and Technology, Atmosphere and Ocean Research Institute (The University of Tokyo), and National Institute for Environmental Studies	MIROC	MIROC-ESM-CHEM

Max-Planck-Institut für Meteorologie (Max Planck Institute for Meteorology)	MPI-M	MPI-ESM-LR
Max-Planck-Institut für Meteorologie (Max Planck Institute for Meteorology)	MPI-M	MPI-ESM-MR
Max-Planck-Institut für Meteorologie (Max Planck Institute for Meteorology)	MPI-M	MPI-ESM-P
Meteorological Research Institute	MRI	MRI-CGCM3
Norwegian Climate Centre	NCC	Nor-ESM1-M
Norwegian Climate Centre	NCC	Nor-ESM1-ME

* The FGOALS-S2 models have been withdrawn from the CMIP5 archive.

Appendix 3.3: Validation Results

A3.3.1 Monsoon Circulations

A3.3.1.1 South West (SW) Monsoon

The SW monsoon brings warm and relatively dry conditions to Singapore during JJAS, while many other regions of south and south-east Asia are receiving the majority of their annual rainfall. While the SW Monsoon circulation is, therefore, not a key direct driver of rainfall for Singapore (rainfall that does occur in Singapore during this season is largely triggered by local convection rather than by large scale circulation features), it does drive the rainfall regimes of many other parts of the region, and the likely knock-on effects of any substantial errors in its representation are likely to have local effects on Singapore.

Figures A3.4 (a, b) show the near surface (850hpa) flow in ERA40 re-analyses and CMIP5 models for which the relevant fields were available. Most models capture the observed broad-scale characteristics i.e. that the occurrence of strongest flow in the core of the Somali Jet is clear, and flow is largely westerly across peninsular India before diverting to a south-westerly flow across the Bay of Bengal, westerly across continental Southeast Asia and finally turning directly southerly before reaching the Philippines. While most models exhibit some variations on these key features, *MIROC-ESM-CHEM* and *MIROC-ESM* both have a monsoon flow which diverts to a southerly flow before reaching continental Southeast Asia, representing a substantial deviation from the patterns observed. The implications of this unrealistic representation of the large-scale characteristics of the SW monsoon in *MIROC-ESM* and *MIROC-ESM-CHEM* is that the represent the characteristics of flow over Southeast Asia are particularly poor – notably, the resulting flow over the South China Sea is predominantly north-westwards instead of north-eastwards as seen in observations. We argue that this significant shortcoming suggests strongly that these models will be unable to represent the potential implications of changes in the SW monsoon on circulation in Southeast Asia (Implausible **-IP**).

The model *inmcm4* has a flow which is significantly weaker than observations throughout the region, although the features are otherwise reasonably realistic (Significant Biases **-SB**), while *IPSL-CM5B-LR* and *MRI-CGCM3* (**SB**) both have a very weak Somali jet combined with flow over southern Asia which is almost directly westerly (compared with observations, where flow diverts south around southern India and becomes south-westerly in the Bay of Bengal).

Other models which demonstrate errors in the circulation are *MIROC5* (flow is directed too southerly over continental Southeast Asia) (Biases **-B**), *ACCESS1-3*, which underestimates the strength of the Somali Jet (**B**), and *FGOALS-g2* and *IPSL-CM5A-LR* all have flow which is particularly too westerly across the Bay of Bengal (B, although we note that there are several other models which offer only a marginal improvement in this characteristic). All GISS models demonstrate a weak Somali jet and substantially too-

strong southerly component of flow into the Bay of Bengal (Not rated as not a model with 6-hourly data available).

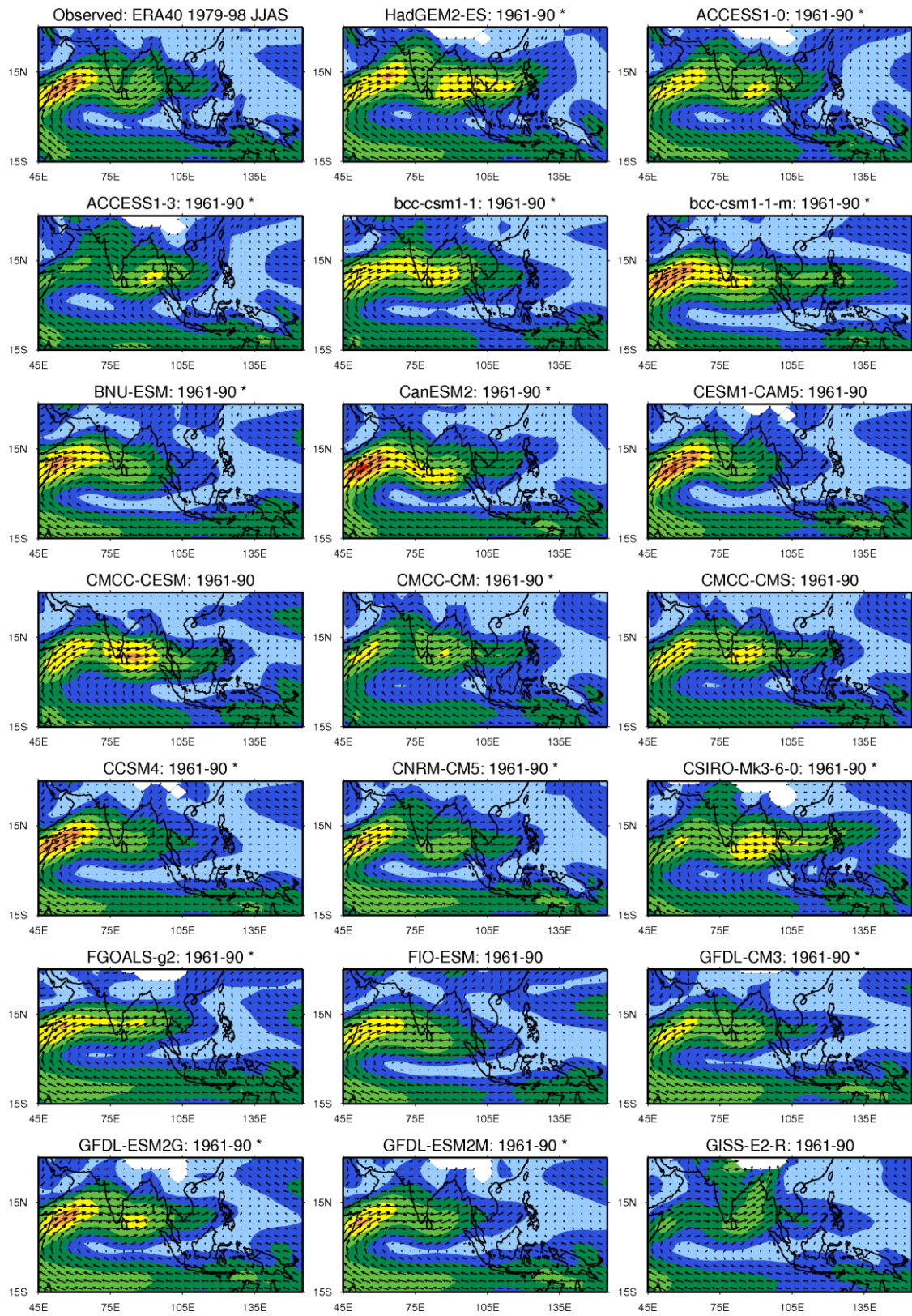


Figure A3.4(a): South-west monsoon circulation (JJAS) in southern Asia in CMIP5 historical simulations and observations from ERA40 reanalyses (Uppala et al., 2005). Starred models are those with 6hourly data available for downscaling.

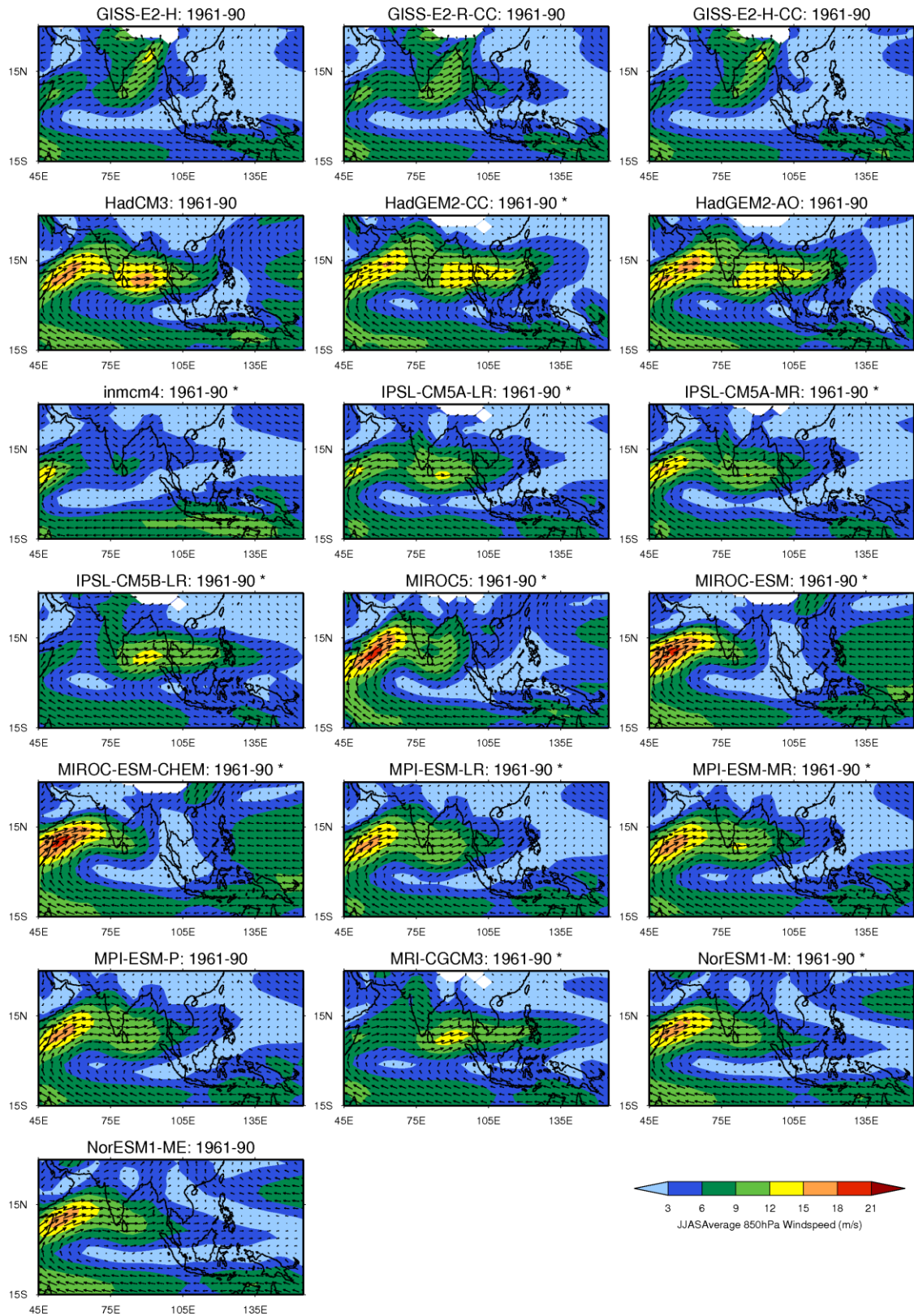


Figure A3.4(b): South-west monsoon circulation (JJAS) in southern Asia in CMIP5 historical simulations and observations from ERA40 reanalyses (Uppala et al, 2005). Starred models are those with 6hourly data available for downscaling.

We also draw on results from the thorough analysis of Sperber et al. (2012), where aspects of both the climatology and the variability of the summer monsoon in a subset of CMIP5 (and CMIP3) models are assessed using a number of performance indices. However, we do not draw on the Sperber et al (2012) indices relating to mean SW monsoon behaviour, because we have already assessed this here. We do however use the indices that summarise other characteristics of the monsoon behaviour, including the relationship between ENSO (Nino3.4) and SW Monsoon intensity (indicated by All-India Rainfall, AIR) , characteristics of the East Asian summer Monsoon, and indices describing the magnitude of variability, and characteristics of the life cycle of intra-seasonal variability (Boreal Summer Intra-seasonal variability BSISV).

The Sperber et al (2012) study assessed whether any of the models were significantly 'better' across a number of these indices by highlighting the highest five values for each index. We have reversed this methodology to identify whether any of the models are significantly worse than others in the ensembles, first identifying those models with the lowest 5 scores across both CMIP3 and CMIP5 ensembles, and then asking (i) are these 'lowest' scores significantly lower than the scores for the majority of other models and (ii) are other scores close to the values found for 'lowest scoring' models, which should therefore be treated similarly? Those models with particularly low scores for any of the indices were assessed as having 'Biases', as errors in their representation of present-day variability of the Monsoon imply that they are unlikely to represent future change in monsoon variability realistically (The limited scope of this study to a sub-set of available CMIP5 models means that we use only the 'Biases' category).

For the Indian Monsoon indices, we found that 5 models scored lowest values for one or both indices (*BCC-CSM-1*, *FGOALS-s2*, *HadGEM2-CC*, *INMCM4*, *MIROC-ESM*, **B**), and additionally 5 other models had scores close to the 'lowest' values (*CanESM2*, *GISS-E2-H*, *MIROC_ESM-CHEM*, *MIROC5*, **B**) (See Table 3.1). For the East Asian indices, only *inmcm4* was significantly lower in its score than other models, entirely failing to capture this aspect of the rainfall variability associated with the East Asian Monsoon (**B**). For the 850hpa wind indices, the lowest scores were not substantially lower than the values scored by other models. The BSISV values were lowest for *MIROC-ESM* and *MIROC-ESM-CHEM* (**B**).

Table 3.1: Indices of summer monsoon variability for CMIP5 models from Sperber et al., 2012. Values in dark blue are those which lie in the lowest 5 across all CMIP3 and CMIP5 models studied, values in light blue were close to those found in the 'lowest' models. Highlighted in yellow are those models which were allocated a 'Biases' rating as a result of these indices.

Indices:

AIR/N34: Correlation between anomalies of Nino3.4 index and All-India rainfall.

Pr Pattern Corr: Spatial correlation of JJAS precipitation anomalies obtained from regression with the Nino3.4 SST.

E.Asian Pr: Negative of Wang-Fan zonal wind shear index regressed against JJA precipitation anomalies.

E.Asian 850hpa: Negative of Wang-Fan (1999) zonal wind shear index regressed against JJA 850hpa wind anomalies.

Boreal Summer Intraseasonal Variance: Pattern correlation of JJAS 20-100 day bandpass filtered Outgoing Longwave Radiation (OLR) variance of observations (AVHRR, 1979-2006) and model (1961-1999).

Boreal Summer Intraseasonal Life Cycle: Spatio-temporal correlation between models and observations of JJAS 20-100day filtered OLR (for a more detailed description of the calculation of the index see Sperber et al, 2012).

	Indian Monsoon		E. Asian Summer Monsoon		Boreal Summer Intraseasonal	
	<i>AIR/N34</i>	<i>Pr pattern corr</i>	<i>Pr</i>	<i>850hpa</i>	<i>Variance</i>	<i>Life Cycle</i>
Observations	-0.533	0.798	0.959	0.989	0.995	0.893
BCC-CSM-1	-0.250	-0.140	0.695	0.93		
CanESM2	-0.273	0.014	0.672	0.861	0.846	0.651
CCSM4	-0.556	0.337	0.789	0.947		
CNRM-CM5	-0.307	0.245	0.642	0.894		
CSIRO-Mk3.6.0	-0.487	0.162	0.346	0.858	0.809	0.645
FGOALS-g2	-0.052	0.238	0.739	0.936		
FGOALS-s2	0.114	0.096	0.787	0.921	0.734	0.608
GFDL-CM3	-0.442	0.192	0.315	0.867		
GFDL-ESM2G	-0.289	0.251	0.458	0.972	0.753	0.643
GFDL-ESM2M	-0.187	0.251	0.606	0.955		
GISS-E2-H	-0.094	0.254	0.586	0.918		
GISS-E2-R	-0.366	0.379	0.656	0.906		
HadCM3	-0.299	0.180	0.773	0.897		
HadGEM2-CC	-0.335	-0.068	0.787	0.935	0.857	0.641
HadGEM2-ES	-0.344	0.216	0.839	0.949	0.862	0.651
INM-CM4	-0.033	0.110	-0.047	0.816	0.639	0.562
IPSL-CM5A-LR	-0.700	0.611	0.450	0.708	0.791	0.654
IPSL-CM5A-MR	-0.763	0.636	0.532	0.749	0.827	0.635
MIROC-ESM	0.088	0.061	0.596	0.694	0.548	0.516
MIROC-ESM-CHEM	-0.104	0.045	0.687	0.882	0.554	0.528
MIROC4h	-0.327	0.529	0.723	0.921	0.736	0.625
MIROC5	-0.321	0.010	0.567	0.946	0.805	0.691
MPI-ESM-LR	-0.291	0.401	0.283	0.899	0.874	0.681
MRI-CGCM3	-0.274	0.338	0.819	0.937	0.782	0.628
NorESM1-M	-0.690	0.522	0.811	0.959	0.833	0.627

A3.1.2 North East (NE) Monsoon

The NE Monsoon perhaps holds greater significance locally for Singapore and the Malaysian peninsula, driving peaks in annual rainfall during November, December and January. ‘Cold surges’, which bring several sequential days of heavy rainfall to Singapore, are associated with this monsoon circulation and have significant impacts on Singapore.

The climatology of the NE Monsoon is assessed by comparing the multi-annual NDJ mean 850hpa flow and pressure anomalies in each model with observations from ERA40 reanalyses and HadSLP2 (Figure A3.5). A key detail of this circulation for Singapore is the north-easterly flow over the South China Sea directing near-surface flow towards the Malaysian Peninsula, and then converging near the equator with the westerly winds from the Indian Ocean. In some of the CMIP5 models, the flow in the north has too strong an easterly component, such that flow is directed more towards the coast of Vietnam rather than further south towards the Malaysian Peninsula – this is particularly true of the models *inmcm4*, *MIROC-ESM*, *MIROC-ESM-CHEM*, *NorESM-1-M* and *NorESM-ME* (**SB**), and, to a lesser extent, *CCSM4*, *CNRM-CM5*, *HadGEM2-ES* and *HadGEM2-CC* (**B**). The ‘Significant Biases’ and ‘Biases’ categories are used here because although important locally for Singapore, this characteristic of the flow may be corrected to some degree in the higher-resolution RCM simulations.

The ‘cold surges’ mentioned above are characterised by pulses of strong north-easterly winds during the NE monsoon over the South China Sea, originating from outbreaks of cold and dry air from the Siberian High (Chang et al., 2005). They last from a few days to a week or more and bring sustained convection over the Maritime Continent that can have dramatic local impacts, such as the 2006/2007 flood event over Peninsular Malaysia (Tangang et al., 2008). Cold surge events are also associated with episodes of extreme sea level anomalies that can cause coastal flooding, especially if concomitant with a high tide (Tkalic et al., 2013).

Cold surges remain relatively unstudied in the existing literature; most existing studies are based on understanding observed characteristics, whilst there is a gap in studies addressing their representation in coupled models or the potential changes in the behaviour of cold surges under warming scenarios. The cold-surge is a relatively large-scale feature, and we therefore expect that if captured by the GCMs, it should be identifiable in even those of relatively coarse resolution. The interaction with other local phenomena, such as the Borneo vortex and the MJO, and the topographic influence in setting preferred areas for deep convection, are expected to be better represented in the regional model.

This means that the evaluation of cold surges is potentially a useful sub-selection criterion in GCM baseline behaviour. The shortage of supporting literature, however, means that this is difficult to employ in practice. Without existing knowledge about suitable techniques for identifying and assessing such features in GCMs, the authors do not consider it feasible within the scope of this project to assess these features across the CMIP5 ensemble with sufficient rigor and robustness to use the outcomes for sub-selection.

We have, however, conducted some exploratory analyses of the selected downscaled simulations, and results are discussed in Chapter 4. This provides contextual information for interpreting the projections that is generated for Singapore in the later

project stages. In this work, representation of cold surges characteristics and their future changes are being analysed in GCMs using a cold surge index based on daily 850 hPa winds, based on the algorithm proposed by Chang et al., 2005.

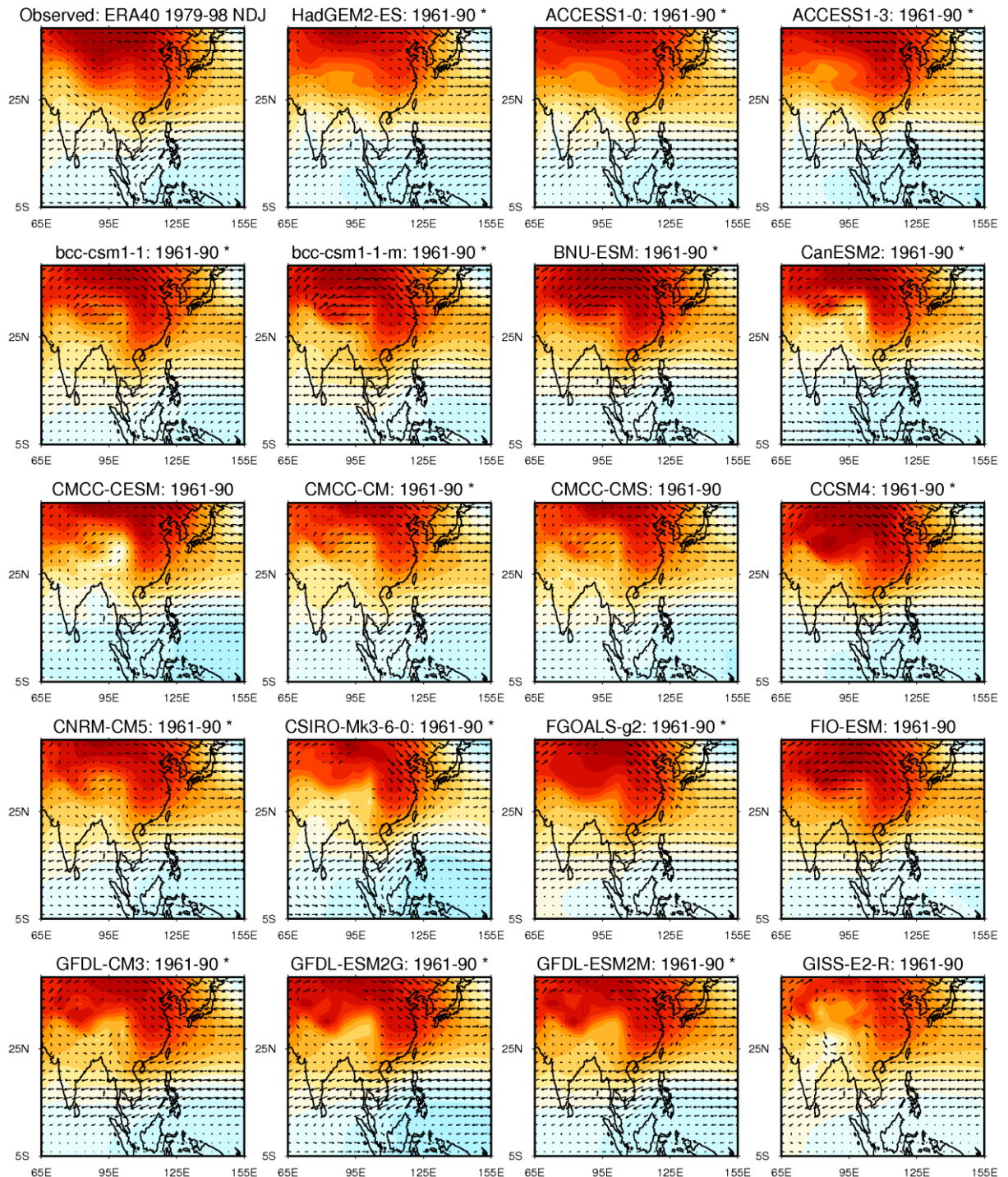


Figure A3.5(a): NDJ 850hpa wind (vectors) and mean sea-level pressure anomaly (colours) for 1961-90 historical simulations from CMIP5 models and observations from ERA40 (Uppala et al, 2003) and HadSLP2 (Allan and Ansell, 2006) and winds and sea-level-pressure respectively. Starred models are those with 6hourly data available for downscaling. See Figure A3.5(b) for colour scale.

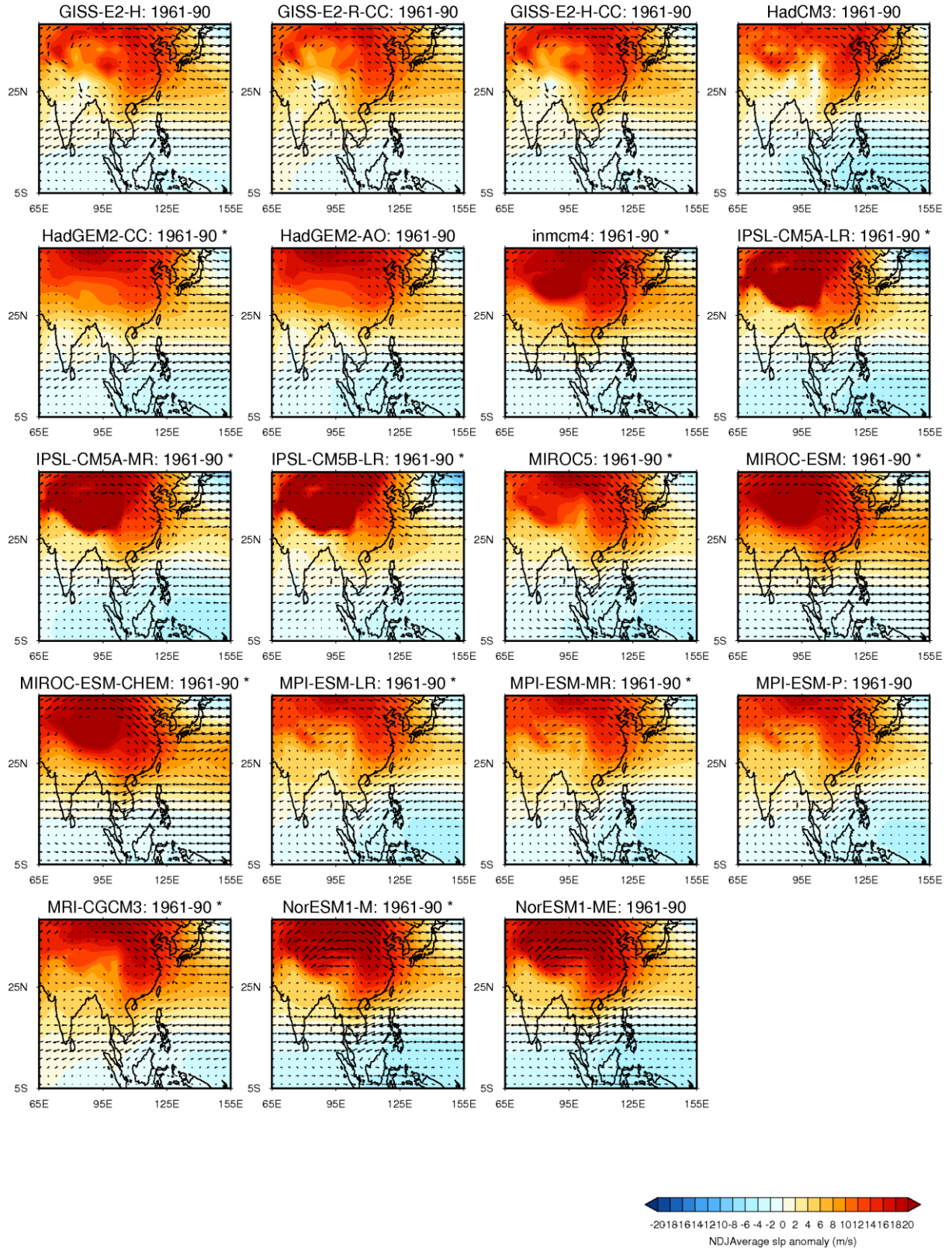


Figure A3.5 (b): NDJ 850hpa wind (vectors) and mean sea-level pressure anomaly (colours) for 1961-90 historical simulations from CMIP5 models and observations from ERA40 (Uppala et al, 2005) and HadSLP2 (Allan and Ansell, 2006) for winds and sea-level-pressure respectively. Starred models are those with 6hourly data available for downscaling.

3.3.2 Seasonal rainfall patterns

The local seasonal cycle of rainfall is determined by a combination of several large scale and local scale processes. Errors in the representation of large scale processes, such as the Monsoon circulation and migration of the ITCZ are likely to be passed to the regional model during downscaling via the LBC data and will therefore affect the higher-resolution downscaled projections similarly to the coarse-scale GCM simulations. The characteristics of local scale processes, like small-scale convective rainfall events, however, are determined largely by the meso-scale processes resolved in the regional model (given realistic large scale conditions), and are likely to be improved by downscaling as a result of the higher-resolution representation of land-surface, topography as well as the atmosphere.

Errors in the simulation of local seasonal cycles diagnosed by the comparison of GCM simulations to gridded observations may therefore result from errors capturing any of a number of large scale processes realistically, as well as from errors in representing the local influences. For the purposes of this sub-selection exercise, in which we are interested in the large-scale errors which would be passed to the regional model, we consider poor performance in the local seasonal rainfall to be an indicator of a potential large-scale error, and therefore use the categories 'Biases' or 'Significant Biases'. We reserve the category 'implausible' for aspects of the large scale climate that are assessed directly.

3.3.2.1 ITCZ migration

Firstly we assess the climatological characteristics of seasonal rainfall across the region by looking at the seasonal migration of the ITCZ in each model (Figure A3.6 a,b).

By visual inspection, we compare the similarity of Hovmoller plots of zonally averaged precipitation in the sector 90-120°E for each model against the GPCPV2.2 observations. An error common to almost all models is an additional band of rainfall in the north at around 25N early in the year (normally in April and May, but in some cases throughout February to August) which can be seen particularly clearly in *ACCESS1-0*, *ACCESS1-3*, all four *GISS* models, *HadGEM2-ES*, *HadGEM2-CC*, *HadGEM2-AO*, *NorESM1-ME* and *NorESM1-M*. In some cases, such as *NorESM1-ME* and *Nor-ESM1-M*, this additional rainfall band in the northern hemisphere is superimposed on a pattern which is otherwise realistic (i.e. the band of summer monsoon rainfall covers a realistic time span, the seasonal northward and southward migrations occur at approximately the correct times of year, and the magnitude of the rainfall is close to observed). In other models, however, such as the *GISS* models, the Northern Hemisphere rainfall error is a more dominant feature of the rainfall pattern. Because the Northern Hemisphere rainfall error is common to a large proportion of models, we do not use this feature in isolation to rate the models.

A characteristic of the ITCZ's seasonal progression is its asymmetric nature, in which the region of maximum convection follows a gradual south-eastward migration path from the Asian Summer Monsoon to the Asian Winter Monsoon, but a sudden transition in the opposite direction (Chang et al., 2005). Instead of reproducing this sudden northward transition during boreal spring, several models demonstrate a

widening of the ITCZ during the summer months (i.e. the equatorial region remains too wet during June-August). This pattern is common to *CMCC-CESM*, *CSIRO-MK3-6-0*, *EC-EARTH*, *GFDL-ESM2G*, *GFDL-ESM2M*, *HadCM3*, *inmcm4*, *IPSL-CM5A-LR*, *IPSL-CM5A-MR*, *MIROC-ESM*, *MIROC-ESM-CHEM*, *MIROC5*, *MPI-ESM-LR*, *MPI-ESM-MR* and *MPI-ESM-P* (B). Conversely, the models *bcc_csm1*, *MRI-CGCM3* and *IPSL-CM5B-LR* have bands of rainfall which are too narrow throughout most of the year (B). *FGOALS-s2* has very weak rainfall in the early part of the year (Jan-Apr) (B).

Models which are rated with ‘significant biases’ show a combination of errors, or an overall pattern which is unrealistic. These are four GISS models (extreme Northern Hemisphere rainfall error), *MIROC-ESM*, *MIROC-ESM-CHEM* (fails to show appropriate seasonal migration, and does not reach the northernmost extent), *MIROC5* (ITCZ too uniform throughout the year except through an extreme Northern Hemisphere rainfall error) and *EC-Earth* (weak seasonal movement) (SB).

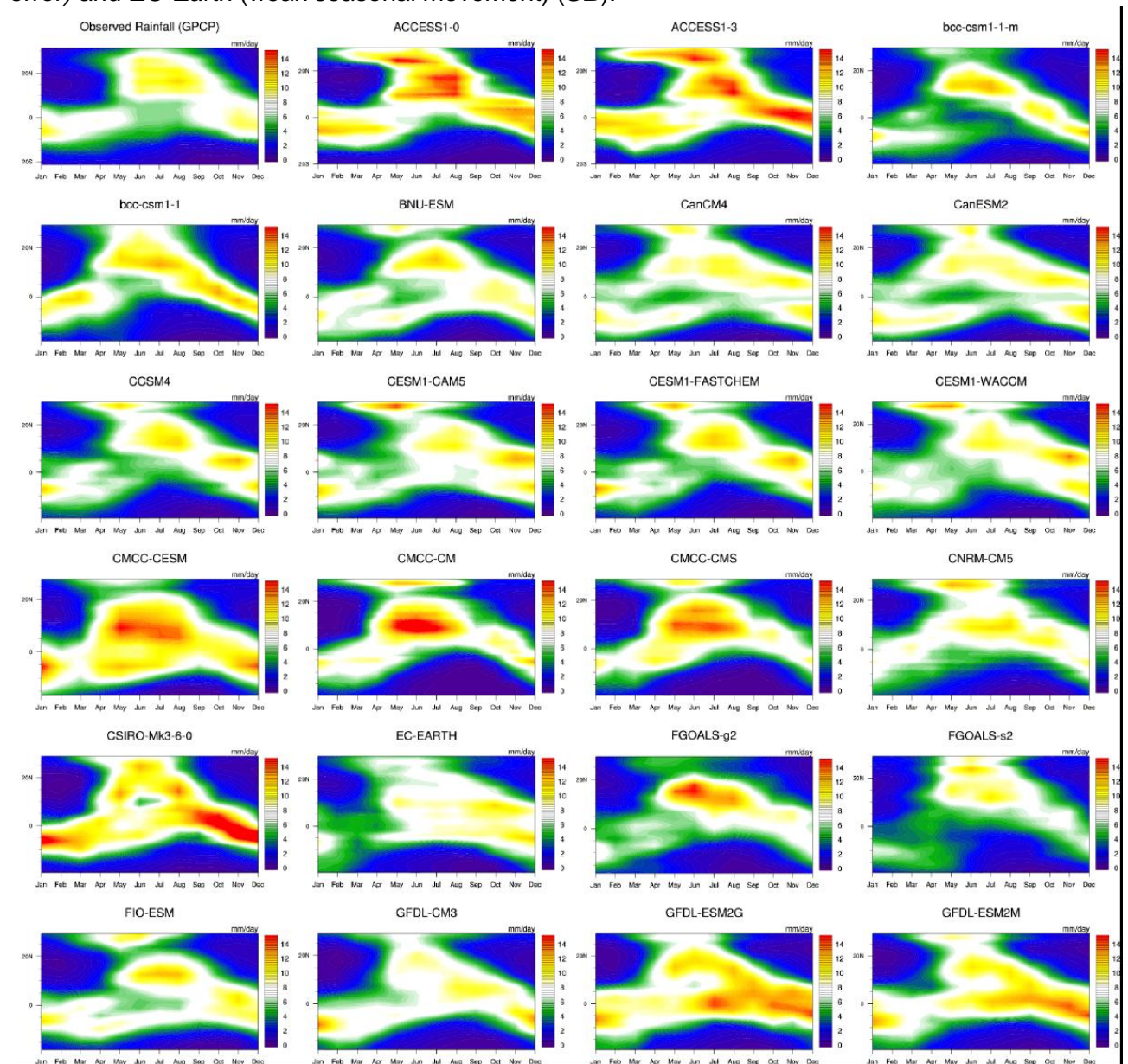


Figure A3.6(a): Hovmöller plots of mean monthly rainfall, 1979 to 2005, for the region 90E-120E and 30N-20S. The datasets were also set to a common calendar (360 days) and also the same reference

time to ensure time periods assessed across models are consistent. Prior to generating the plots using the NCL both the GCM and GPCP (Adler *et al.*, 2003) datasets had been re-gridded to a common grid using linear interpolation.

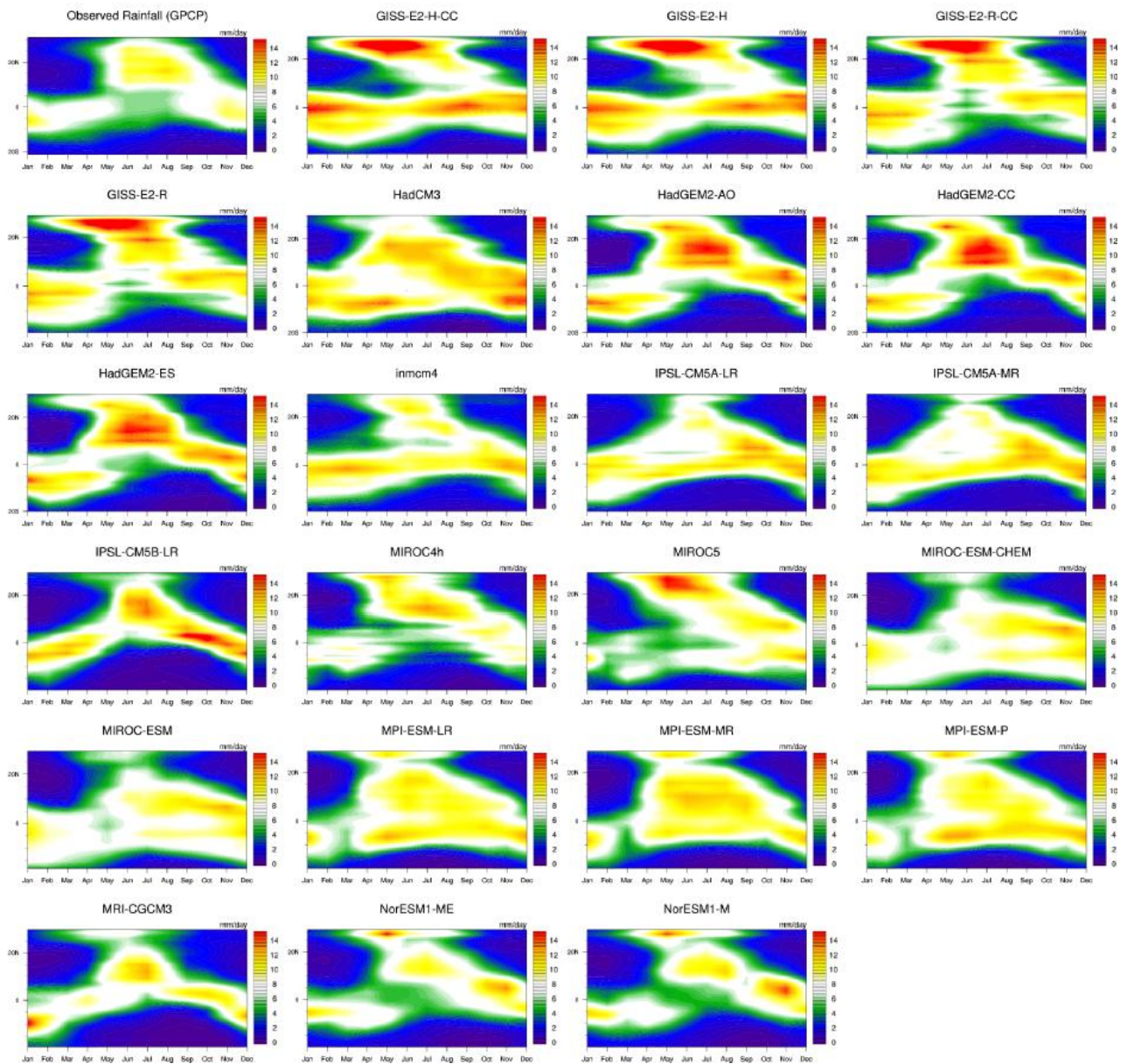


Figure A3.6(b): Hovmöller plots of mean monthly rainfall, 1979 to 2005, for the region 90E-120E and 30N-20S. The datasets were also set to a common calendar (360 days) and also the same reference time to ensure time periods assessed across models are consistent. Prior to generating the plots using NCL tools both the GCM and GPCP (Adler *et al.*, 2003) datasets had been re-gridded to a common grid using linear interpolation.

3.3.2.2 Annual rainfall cycles

We assess the climatological seasonal rainfall patterns over the set of smaller specific regions shown in Figure A3.7, as well as for the wider region of south-east Asia (SEA). The sub-regions are organised according to their climatology and a brief discussion of this is provided in Appendix 4. We plot every model for which data is available together, but use performance indices to identify the ‘worst’ models, which are highlighted for inspection. This approach allows us to use indices to pull out the least well performing models, whilst also allowing us to make our own judgements on whether those models are significantly worse than others. The metrics used are *RMSE* of the 12 monthly values, and *r*, the correlation between the 12 monthly values between each model and the observed dataset. Any model which lies in the lowest 10 values across all models assessed (including those for which LBC data are not available) for either metric are highlighted in Figure A3.7.

For some regions the models have more difficulty in capturing the seasonal cycle than others – this is particularly true of the Malaysian Peninsula and Sumatra and Borneo regions which have more complex seasonal cycles than the more northern and southern regions. For the northern regions of continental SEA, and the Philippines, the models generally capture the timing and magnitude of the Monsoon rainfall in JJAS with reasonable skill. An exception to this are the 3 *MIROC* models (**B**), which all suffer from very late rainy season onset in the Philippines (SON is the wettest period for these models, rather than JJAS). *GFDL-ESM2G*, *GFDL-ESM2-M* and *MRI-ESM-MR* feature an additional peak in rainfall in this late season also (**B**). *IPSL-CM5B-LR* suffers significantly late onset of the Monsoon rainfall over Continental SEA (**B**). In the southern regions of Java and New Guinea, most models capture the reversed annual rainfall cycle, with JJAS as the driest season, although many have a more pronounced seasonality than observations with wetter DJF than observed. As this is a feature common to many models we do not give B/SB ratings. The *MIROC-ESM* and *MIROC-ESM-CHEM* models are again exceptions to this, with a very subdued annual cycle over Java (**SB**, due to poor performance across multiple regions). The varied realism in the representation of the seasonal cycle of rainfall across the regions is not surprising given the differences in the representation of the progression of the ITCZ and Monsoon circulations identified sections in 4.1 and 4.2.1. *MPI-ESM-LR* also displays an additional rainfall peak in May and June (**B**).

For the equatorial regions of the Malaysian Peninsula and Sumatra and Borneo, performance varies more between models. Both *MPI-ESM-LR* and *MPI-ESM-MR*, as well as *CMCC-CM* fail to capture the observed characteristics of the annual cycle, showing peak rainfall during June-October, which are the driest months in observations (**SB**). *GFDL-ESM2G* and *GFDL-ESM2M* have a tendency to be fairly consistently too wet throughout the year (**B**), although they broadly capture the seasonal cycle. *Inmcm4* also fails to capture the seasonal cycle over Malaysian Peninsula and Sumatra, with considerably more rainfall than observed during Feb-May (**SB**). While *CSIRO-mk3-6-0* tends to have excessive rainfall maxima, they do occur at the correct time of year so we do not use a B rating.

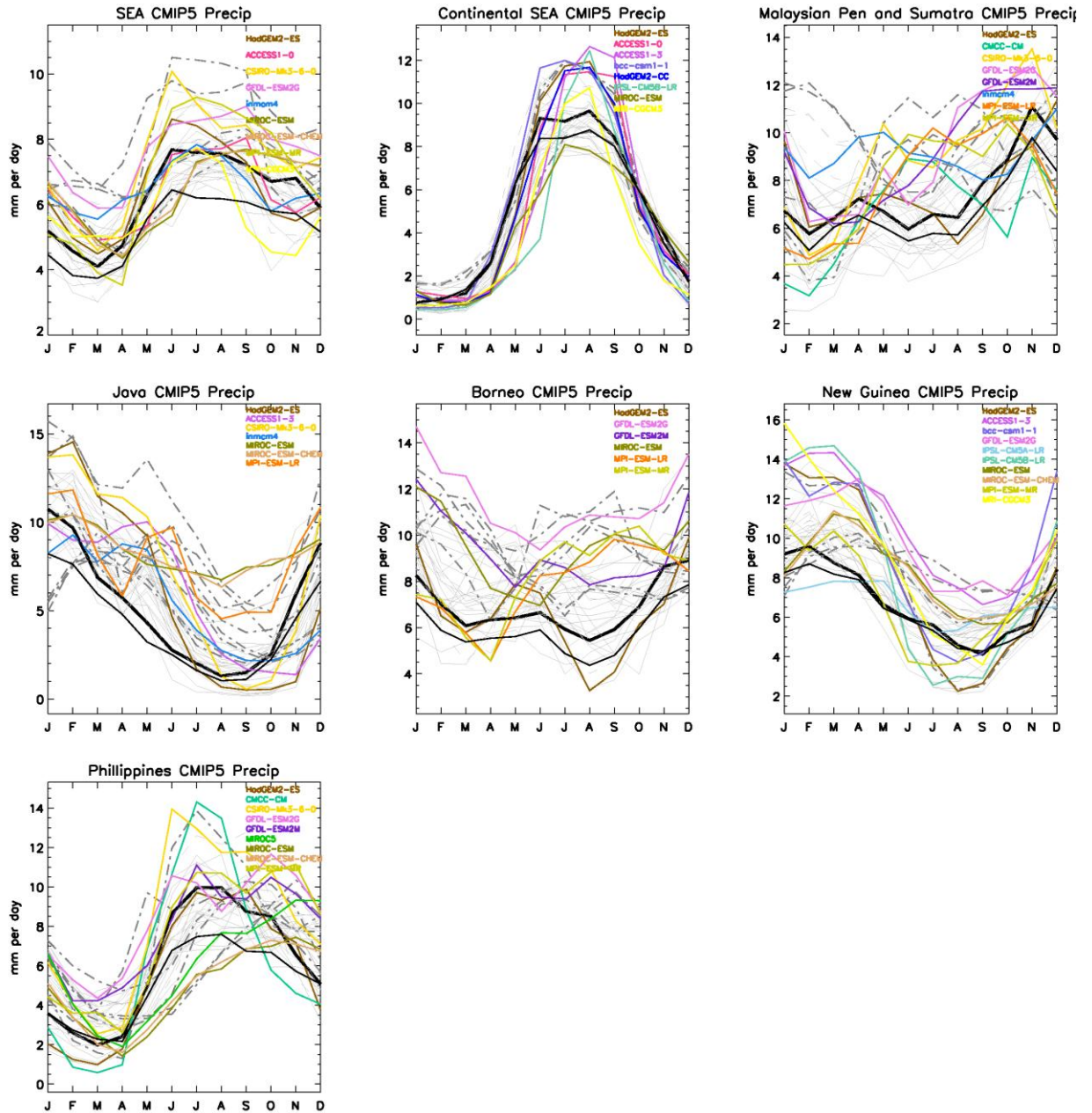


Figure A3.7: Annual cycles of area-averaged rainfall 1961-90 in CMIP5 models for Southeast Asia sub-regions depicted in Figure A3.8. Coloured lines indicate those with $RMSE$ or r scores in the lowest 10 for each region. Dotted and dot-dashed lines are those for which LBC data are not available. Black lines are observations from GPCP (Adler *et al*, 2003) (heavy line) and CMAP (Xie and Arkin, 1997) (lighter line) datasets respectively.

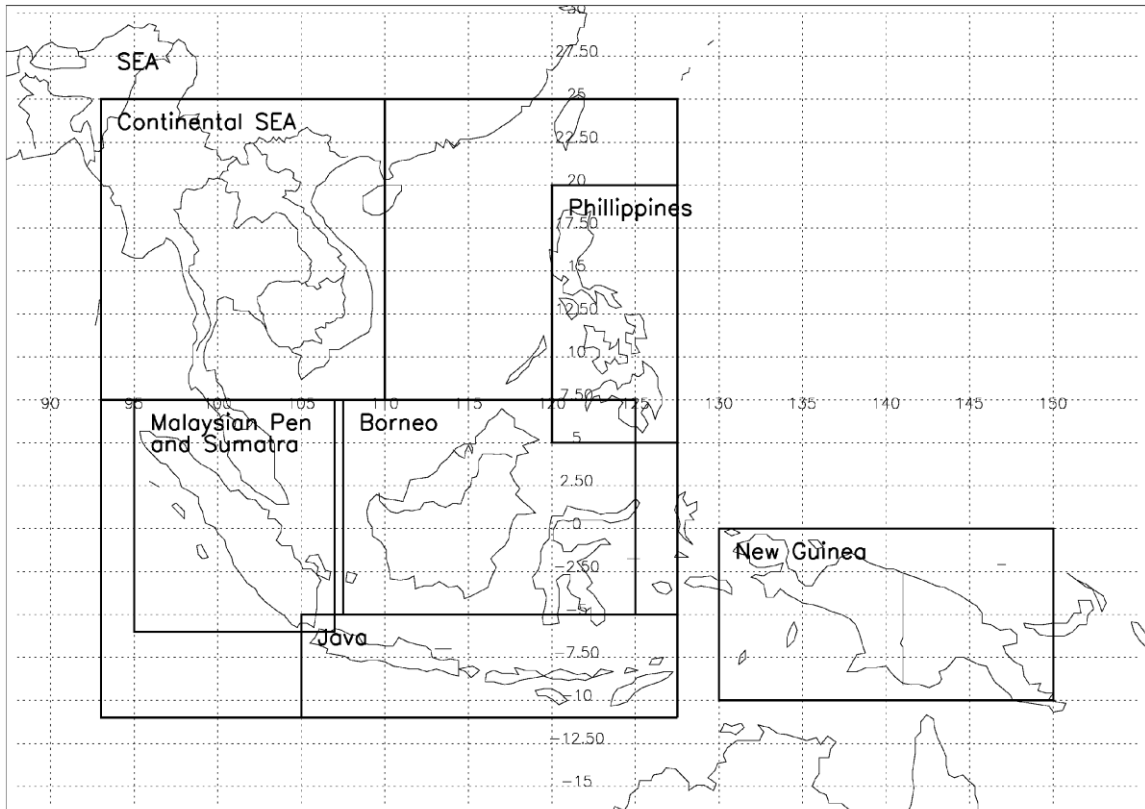


Figure A3.8: Regional definitions used to assess annual cycles of rainfall for key land regions of Southeast Asia.

3.3.3 Sea surface and air temperatures

Sea-surface temperatures, both locally and more remotely, are known to exert a significant influence on the climate of Southeast Asia. A key aspect of this is the ENSO variability, which is known to have strong tele-connections with Southeast Asia which we discuss in Section 4.5. Here we focus on the climatological aspects of SSTs.

Firstly, we assess whether the models capture a realistic seasonal cycle in both SSTs and 1.5m air temperature over land (Figure A3.9). For SSTs, the region we assess is extended into the Pacific in view of its key influences on Southeast Asia. The models tend towards a cool bias throughout the year, particularly during winter months. The largest of the cool biases affect *EC-Earth*, *GFDL-CM3*, *FGOALS-g2*, *MIROC-ESM*, *MIROC-ESM-CHEM* and *NorESm1-M (B)*, at around 1 degree compared with HadISST. While most models capture the annual cycle well in spite of the small biases, three show more significant deviations from the observed, with the relatively warm conditions observed in May-July extending into August-October. The high number of coast points in Southeast Asia means that the differences between the number of land points between models of different resolution mean that these values are not directly comparable. However, it is clear that 2 models suffer from issues of concern – *inmcm4* and *EC-Earth* both demonstrate particularly large cool biases in the air temperature over land. In the case of *EC-Earth*, this is likely to reflect the SST biases, while for *inmcm4*, the cool biases in air temperature over land exceed those in SSTs. By looking at the complete spatial fields of 1.5m temperature (Figure A3.10a,b) we can see that the characteristics

of the errors in *inmcm4* and *EC-Earth* are quite different. The cool bias affecting *inmcm4* evidently only affects the land areas, implying that the source of the error is related the interaction with the land surface, which means that the errors is unlikely to affect RCM simulations driven by this GCM (**B**). However, in the case of *EC-Earth*, the error is considerably amplified in the air temperature directly over the ocean compared with the sea-surface temperature. This presents a more significant large-scale error, whereby the model suffers not only a significant temperature bias, but also a mismatch in the relative temperatures of the sea-surface and the air directly above it (**SB**).

Secondly we assess the spatial patterns of SSTs (Figure A3.11a,b). An error common to many GCMs is the ‘cold tongue’ bias in the eastern pacific (Riechler and Kim, 2008; Hirota and Takayabu, In Review), where by the relatively cool region of the equatorial east pacific extends too far west. Errors in SST are known to propagate readily throughout the free atmosphere (Riechler and Kim, 2008), having significant impacts directly on the air temperature and rainfall patterns (e.g. Hirota and Takayabu, In review).

In Figure A3.11 we show a cold-tongue index (CT) proposed by Hirota and Takayabu (In review), which is defined as the difference between the SST anomaly from the average over the whole tropical ocean averaged over the region 3S to 3N, 180W, 150W. According to this index, *CSIRO-mk3-6-0* (**SB**) clearly suffers the largest cold-tongue bias. However, we note that by visual inspection, 2 other models have similarly large cold tongue biases which are not well captured by the CT index - *inmcm4* and *HadCM3* (**SB**).

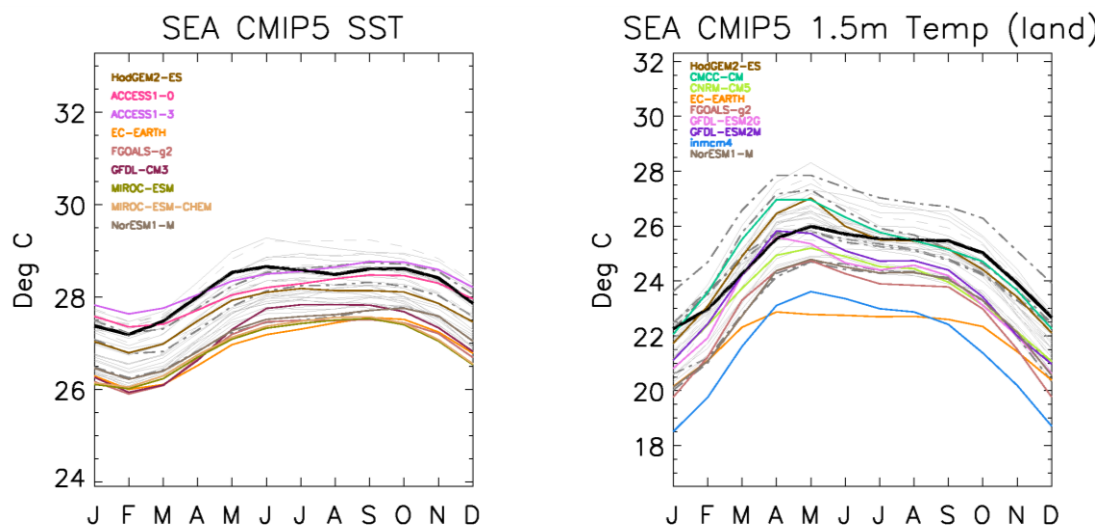


Figure A3.9: Extended-SEA region annual cycles of Sea-Surface temperature for ocean points (left) and land points (right). Black lines indicate observed data from HadISST (Rayner et al., 2003) and CRU (Mitchell and Jones, 2005) datasets respectively. Coloured lines indicate those CMIP5 models with *RMSE* or *r* scores in the lowest 10 for each region. Dotted and dot-dashed lines represent models for which LBC data are not available. Extended SEA region is defined as 11S-25N and 93E-180E.

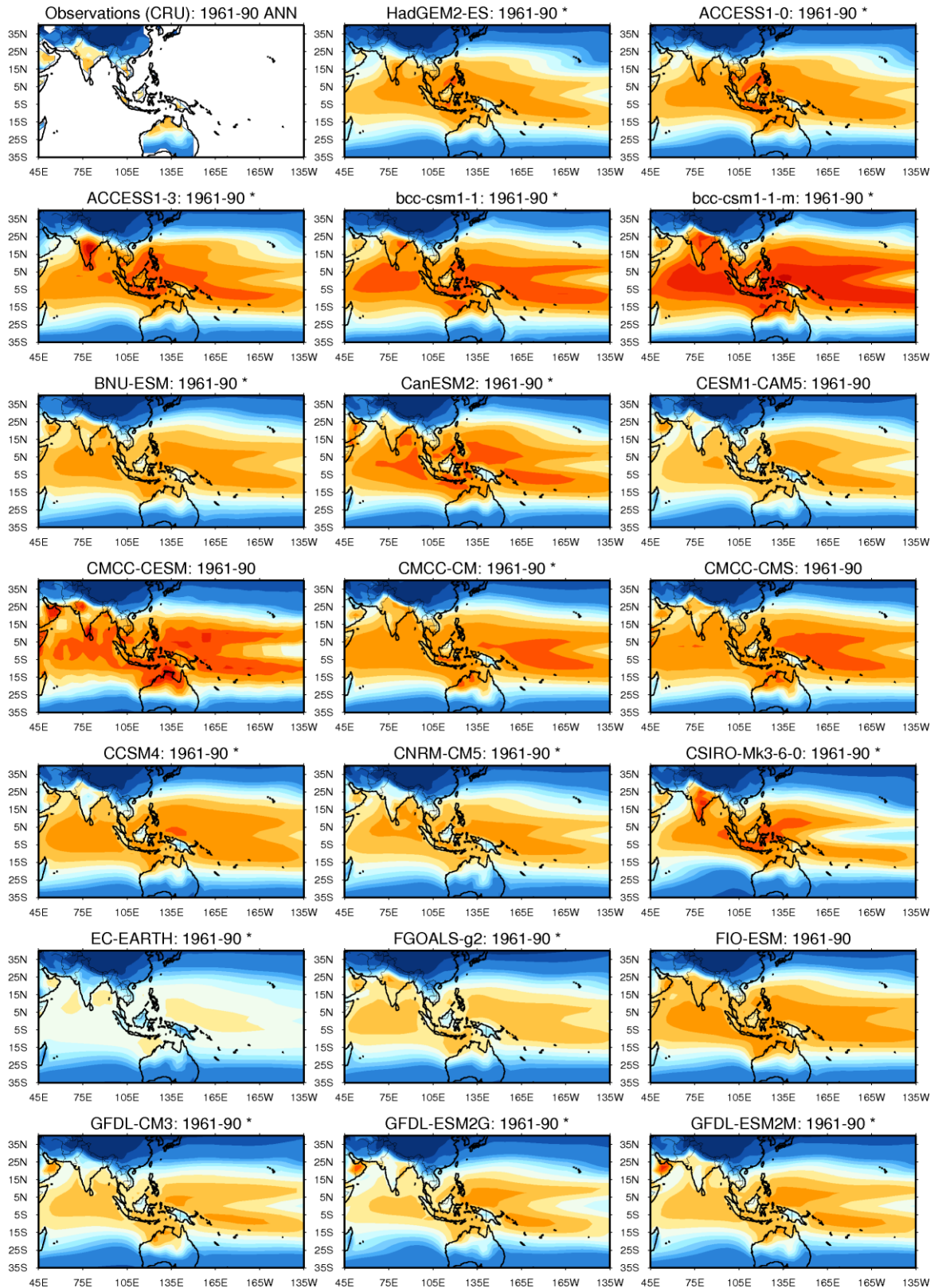


Figure A3.10(a): 1.5m air temperature in CMIP5 historical simulations and CRU gridded temperature observations (land only) (Mitchell and Jones, 2005) – Annual mean.

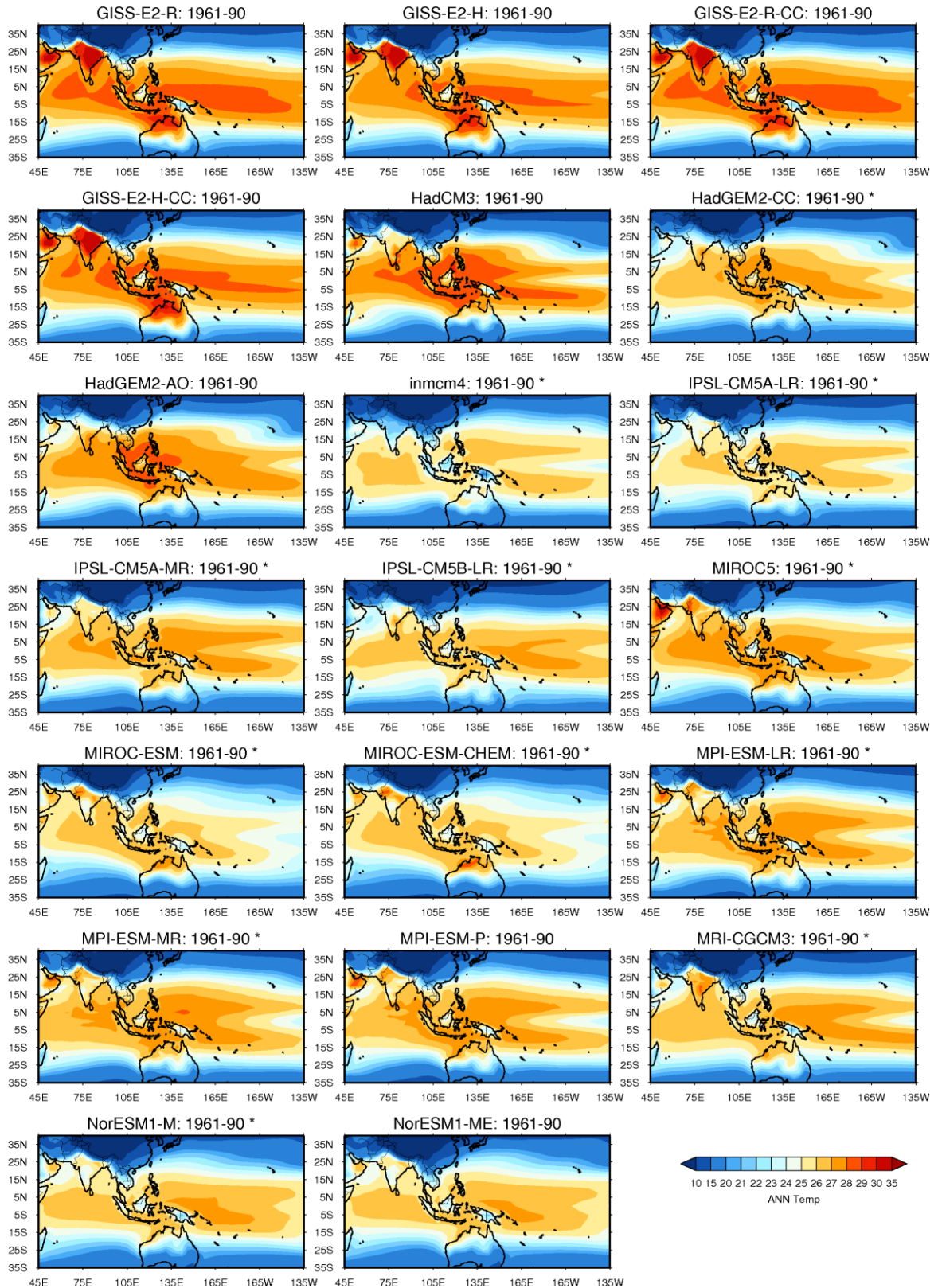


Figure A3.10(b): 1.5m air temperature in CMIP5 historical simulations and CRU gridded temperature observations (land only) (Mitchell and Jones, 2005) – Annual mean.

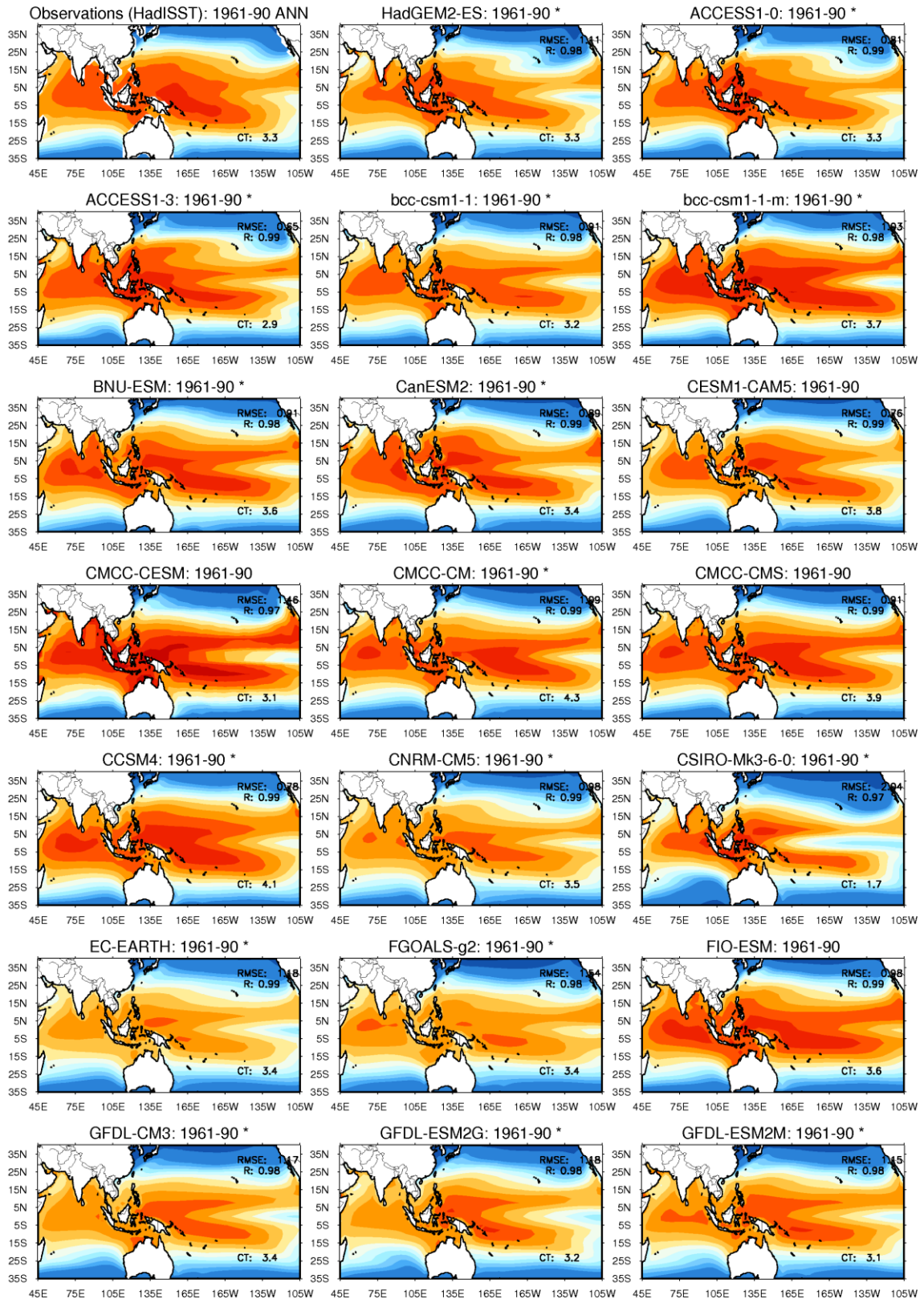


Figure A3.11(a): Sea-surface temperatures in CMIP5 historical runs and HadISST2 observed gridded dataset – Annual mean. The root-mean square error (RMSE), spatial correlation of model values with HadISST (Rayner et al, 2003) observations (R) and the cold tongue Index (CT, Hirota and Takayabu, In review) are given for all models.

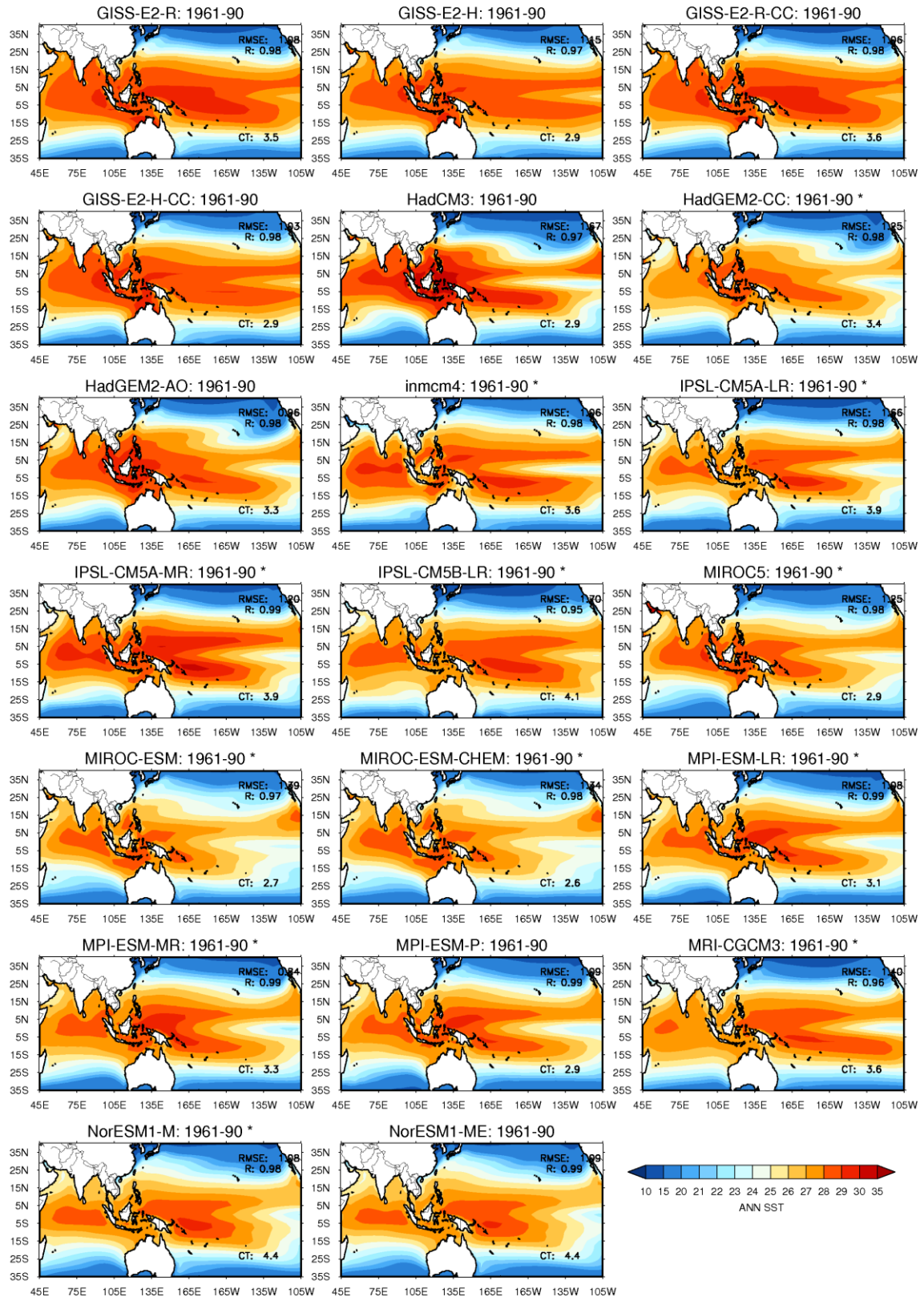


Figure A3.11(b): Sea-surface temperatures in CMIP5 historical runs and HadISST2 observed gridded dataset – Annual mean. The root-mean square error (RMSE), spatial correlation of model values with HadISST (Rayner et al., 2003) observations (R) and the cold tongue Index (CT, Hirota and Takayabu, In review) are given for all models.

3.4 Key Modes of Variability

3.4.1 ENSO and tele-connections in Southeast Asia

The El-Nino Southern Oscillation (ENSO) is known to exert a strong influence on the Southeast Asia region, both via an observed direct correlation between mean rainfall across the region and via a well-established observed relationship between ENSO and the south-west Monsoon intensity (see, for example, Lim et al., 2007; Hu et al., 2005).

An assessment of the representation of the negative correlation between the Nino3.4 index and All-India rainfall (as an index of SW monsoon intensity) included in the suite of indices assessed by Sperber et al. (2012) has already been accounted for in our assessment of SW monsoon variability in Section 4.1.1, and further assessments of the direct tele-connection between monthly rainfall anomalies and Nino3.4 across Southeast Asia (not shown) yielded performance results that were highly correlated with those of the Sperber et al Nino3.4/AIR index. Both of these sets of analyses demonstrate that most models correctly simulate a negative relationship between Nino3.4 and SW monsoon rainfall (*FGOALS-s2*, *MIROC-ESM* are exceptions to this), though in most cases this relationship is too weak.

For an assessment of ENSO itself, we draw on a number of published studies which systematically assess its behaviour across the CMIP5 ensemble. Guilyardi et al (2012) and, in greater detail, Bellenger *et al.* (In Press) assess in CMIP5 models a number of metrics of ENSO amplitude (NINO3 SST standard deviation), structure (Nino3 vs Nino4 amplitude), frequency (Root Mean Square Error, RMSE, of Nino3 SSTA spectra) and heating source (Nino4 precipitation standard deviation). Several process-based metrics are also assessed in these papers, which reflect the role of the atmosphere response to ENSO, and therefore represent an assessment of whether the models capture the key processes required to represent ENSO realistically. Guilyardi et al. note that a significant improvement in the ENSO amplitude and frequency in CMIP5 compared with CMIP3, but little change in heating source, or the mean state metrics examined. While the simulated amplitude of SST variability may have converged towards observed values since CMIP3, the process-based indices assessed show no such improvement, indicating that the apparent improvement in this metric may not reflect a genuine improvement in ENSO realism. Guilyardi et al. speculate that the apparent improvements may reflect an increase in tuning towards more realistic ENSO characteristics.

While the realistic representation of the atmospheric feedback processes is clearly important in determining a model's suitability for process-based studies of ENSO, the use of the models to explore the models' ENSO responses to external forcing require both the realistic representation of both underlying key processes and emergent ENSO characteristics in order for us to be able to diagnose changes in ENSO characteristics. Only a very small number of CMIP5 models (CNRM-CM5, FGOALS-g2, CCSM4 and GFDL-ESM2M) meet these criteria due to the larger number of models which perform poorly on the process-based metrics (Guilyardi et al.,2012). For studies that are focussed specifically on ENSO responses, the small subset of models which simulate both the processes and ENSO characteristics realistically may be a useful means of studying changes in ENSO. In the context of this study, however, where we are interested in exploring and understanding changes in climate for the region more

broadly, such that a restricted subset does not provide a good basis for understanding the range of projected changes in other aspects of climate change in the region. We therefore only use the metrics representing emergent ENSO characteristics, published in Guilyardi et al., 2012, and Bellenger et al., *In press*) only as a basis for informing sub-selection. On this basis, 6 of the 33 CMIP5 models assessed demonstrate significant shortcomings in their representation of one or more aspects across the four characteristics of ENSO: *CMCC-CM*, *CSIRO-mk3-6-0*, *FGOALS-s2*, *inmcm4*, *MIROC-ESM*, and *MIROC-ESM-CHEM (B)*.

A notable issue is that *CSIRO-mk3-6-0* demonstrates unrealistic structure, with higher variability in the west than the east pacific, the reverse of observations and all other CMIP5 models assessed (one other CMIP3 model demonstrated this feature also). This feature of *CSIRO-mk3-6-0* is also noted by Kim and Yu (2012) in their assessment of the relative intensities of east and central pacific El-Nino events, and lies beyond the range of errors in the other 19 models assessed.

A further study (Zhang and Jin, 2012) assesses the bias in meridional width of ENSO SST anomalies. SST anomalies in coupled GCMs tend to be too tightly confined to the equator, which is demonstrated to have a significant impact on the ENSO precipitation response over the eastern tropical Pacific (Zhang and Jin, 2012). Of the 16 CMIP5 models assessed in this study, all displayed a negative bias in meridional width, with models *CanESM2*, *CNRM-CM5*, *GISS-E2-H*, *inmcm4*, and *NorESM1* demonstrating the largest biases. However, as this bias is common to all models assessed, and the 'worst' biases are not substantially more than the rest of the ensemble, and the information is available for only 12 of the 29 models in which are most interested, we do not score the models explicitly based on this criterion.

3.4.2 Madden-Julian Oscillation (MJO)

The MJO is a key aspect of intra-seasonal variability affecting Southeast Asia and across the tropics, influencing onset and breaks of monsoon systems, formation of tropical cyclones and, on longer timescales, the triggering and termination of ENSO events (Hung et al, 2013).

Historically, GCMs have not represented MJO variability well – Lin et al, 2006, found that only 2 of 14 CMIP3 models assessed had MJO variance comparable to observations. Exploratory work (e.g. Kim et al, 2011) has shown that a conflict exists between the improvement of MJO variability and maintaining a realistic mean base state, and that parameterization changes which improve the MJO simulations may have been rejected due to the corresponding degradation in mean state (Kim et al, *Submitted*).

Studies of MJO variability in CMIP5 have indicated that some models show a notable improvement over CMIP3 in their representation of MJO variance, while other aspects of the feature, such as the eastwards propagation, remain poorly simulated in all but one model (*CNRM-CM5*) (Hung et al, 2013). Kim et al (*Submitted*) present a number of indices reflecting the realism of the MJO in each model, which we have extended to include all CMIP5 models for which the daily precipitation fields were available (Table 3.2). These indices represent two different aspects of MJO behaviour: 'East-West' is the ratio of eastward to westward power at MJO time and space scales indicating how prominent the MJO is compared to background variability; 'East' is, more simply, the power summed over eastward waves at the same space and timescales, giving a direct indication of the magnitude of eastward power. The two indices are highly correlated

(Figure A3.12), and we therefore identify models which perform the least well over the two indices as *bcc-cms-1-1-m*, *CanESM2*, *CNRM-CM5*, *inmcm4*, *MIROC-ESM* and *MIROC-ESM-CHEM* (**B**).

Data	East/West	East
GPCP	2.20	0.22
TRMM	2.73	0.20
ERA-I	2.09	0.10
ACCESS1-0	1.41	0.05
ACCESS1-3	2.02	0.07
bcc-csm1-1	2.93	0.14
<i>bcc-csm1-1-m</i>	0.96	0.06
<i>BNU-ESM</i>	1.60	0.09
<i>CanESM2</i>	0.87	0.03
<i>CMCC-CM</i>	3.05	0.27
<i>CMCC-CMS</i>	2.14	0.25
<i>CNRM-CM5</i>	4.95	0.46
CSIRO-Mk3-6-0	1.70	0.07
FGOALS-g2	2.13	0.07
<i>FGOALS-s2</i>	1.56	0.13
GFDL-ESM2G	1.39	0.06
GFDL-ESM2M	1.26	0.07
<i>IPSL-CM5A-LR</i>	1.59	0.06
<i>inmcm4</i>	1.16	0.03
<i>MIROC-4h</i>	1.62	0.05
<i>MIROC-ESM</i>	0.91	0.04
<i>MIROC-ESM-CHEM</i>	0.65	0.04
MPI-ESM-P	1.34	0.11
<i>MPI-ESM-MR</i>	1.31	0.14
<i>MPI-ESM-LR</i>	1.62	0.19
<i>MRI-CGCM3</i>	3.15	0.25
<i>NorESM1-M</i>	2.64	0.15

Table 3.2: Indices of fidelity of the Madden-Julian Oscillation for observed datasets and CMIP5 models 1978-1998. Values in Italics are taken directly from Kim et al. (Submitted), and indices for additional models were calculated using an identical methodology. Models highlighted in yellow are those rated as ‘Biases’.

East-West: the ratio of eastward to westward power at MJO time and space scales (zonal wavenumbers 1-3 and periods 30-90 days) indicating how prominent the MJO is compared to background variability. **East:** eastward power summed over eastward wave numbers 1-3 and periods 30-90 days. This index does not discriminate between eastwards and westward propagation, but gives a direct indication of the magnitude of eastward power.

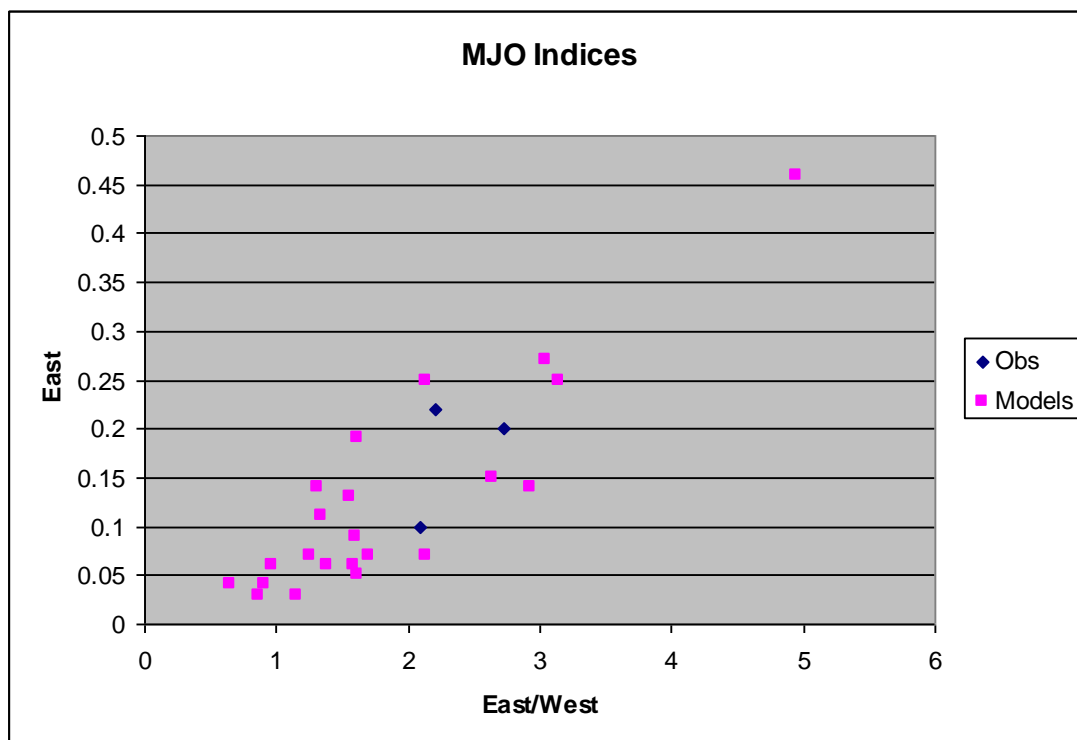


Figure A3.12: Relationship between two indices of the MJO for observed datasets and CMIP5 models, values are listed in Table 3.2.

Appendix 3.4: Tropical Cyclone (TC) assessment methodology

Author: Grace Redmond

TC-like structures were tracked over the North West Pacific in 24 members of the CMIP5 ensemble for both present day historical runs (1971-2002) and future RCP8.5 runs (2064-2095). Firstly, models were eliminated which were not found to be capable of producing reasonable TC like structures (see Method for elimination criteria); and then for those models which can reasonably represent TCs the projected changes in TCs by the end of the century (2064-2095) were examined.

3.4.1 Tracking Methodology

The tracking algorithm used, developed at the Met Office by (Dr.) David Fereday, identifies TCs based on instantaneous daily 850hPa relative vorticity and tracks them in space and time. To be considered a TC, relative vorticity must exceed a vorticity threshold set by the user (which was adjusted according to the CMIP5 member in question to tune historical TC numbers towards observations) and last for a minimum of two time steps (two days). For a list of CMIP5 ensemble members tracked, their associated resolution, relative vorticity threshold used for TC identification and historical number of TCs (1971-2002) see Table A3.1.

It is important to bear in mind that the algorithm re-grids CMIP5 model outputs to a N96 grid (same as HadGEM2-ES), and the re-gridding method applied (bilinear interpolation for those models at a resolution less than N96, and aggregation for those at higher resolution) had an impact on the number of TCs detected. Unfortunately, given time and resource constraints it was not possible to re-write the algorithm in order to track models on their native grids. This algorithm does not apply a warm core test to identify TC like structures; therefore it is possible that other (non-warm core) storm systems are mis-identified as TCs.

Data from the International Best Track Archive for Climate Stewardship (IBTrACS) has been used as an observation data set for validation. IBTrACS data is available online at <http://www.ncdc.noaa.gov/oa/ibtracs/>. A full description of this dataset can be found in Kruk et al. 2010. We have used 1979-2010 IBTrACS observations; however, these observations can not be directly compared to CMIP5 output. IBTrACS identifies TCs based on wind speed thresholds, and is essentially point data, whereas the model uses 850 hPa relative vorticity for identification and data is an area average (therefore we do not expect the intensity of TCs in the models to be comparable to IBTrACS.) We use the observations as a guideline of the spatial distribution of West North Pacific TCs, their annual cycle and estimates of overall TC number.

In order to characterise the changes in TCs under the RCP scenario runs, we examined the changes in the models which were able to reproduce reasonable representations on North West Pacific TCs. The criteria for including a model in the TC analysis is set out below:

Reasonable magnitude of TC like storms (>20% of observations, >160) , so as there are enough storms to carry out meaningful examination of future changes.

Reasonable spatial distribution of tracks – use only models whose TCs in a broadly similar location to observations.

Realistic annual cycle – TC season in the NW Pacific is primarily June-December, if models do not pick up a reasonable number of TCs in this period with respect to the rest of the year then they are not included. Outside of and during TC season there are other North West Pacific storms, but it is rare that these are TCs, however, due to the lack of a warm core test, some models may pick these up as TCs.

3.4.2 Results

Firstly considering the number of TCs simulated by the 24 CMIP5 members in the present day (1971-2002), 12 models failed to meet criteria one (i.e. they produced too few TCs). Table A3.1 contains the number of TCs produced in each of the ensemble members for the historical runs and Figure A3.13 shows the number of TCs in IBTrACS observations (796) for a 32 year period (1979-2010). Those eliminated were FGOALS-s2, GFDL-CM3, GFDL-ESM2M, GFDL-ESM2G, Inmcm4, IPSL-CM5A-LR, IPSL-CM5A-MR, MIROC-ESM, MIROC-ESM-CHEM, MPI-ESM-LR, MPI-ESM-MR and NorESM1-M. All of these models had <100 TCs in 32 years and the tracks often had poor spatial distribution (Figure A3.14), with tracks often being very short.

Of the 12 ensemble members remaining, all had a reasonable spatial distribution of tracks over the North West Pacific as seen in Figure A3.14, which shows the tracks from all 24 ensemble members for the historical period. Although certain ensemble members show tracks that are often shorter and more erratic than in observations, and in the case

of IPSL-CM5B-LR primarily in a north-south direction instead of east-west as is more commonly observed. No further models were excluded solely on the grounds of criteria two.

Criteria three states that the models should have a reasonable representation of the annual cycle of North West Pacific, with the majority of TC activity occurring between June and December, governed by the Southwest monsoon between June and September and the Northeast monsoon from October to December. Figure A3.13 shows the IBTrACS annual cycle which peaks in August and is at a minimum in January and February. Figure A3.15 shows the annual cycle of all 24 CMIP5 members considered. Of the 12 ensemble members which satisfy criteria one and two, 5 had a poor annual cycle, with very few TCs particularly during the June- November period, but a large number in January-April. Those models are bcc-csm1-1, CSIRO-Mk3-6-0, FGOALS-g2, IPSL-CM5B-LR and MIROC5. It is possible that these 8 models are in fact failing to generate TCs, but are able to produce relative vorticity maxima associated with North West Pacific storms, although this has not been investigated further. The other 8 models have a reasonable representation of the annual cycle of TCs in this region, the only border line model in CanESM2, which peaks in December and has a significant number of TCs in January, however it has few between February and April and more than 50 in each month from June-December so on this basis it was included.

Intensity of the average maximum 850hPa wind speed reached by TCs in each of the 24 models was also assessed; this can be seen in Figure A3.16. Despite their varying resolutions, all ensemble members had comparable maximum TC wind speeds, ranging from 20-28m/s. We did not compare these with observations given the limitations of comparing point data and area averages. Figure A3.17 shows the spatial distribution of TCs 2064-2095, which looks very similar to present day TC distribution in Figure A3.14. However, projections in the number of TCs varies across the ensemble members, 5 project a decrease in the number of TCs and 2 project an increase (bcc-csm1-1-m and MRI-CGCM3), these results can be seen in Figure A3.18a, with a range of -49% to 20% . As shown in Figure A3.18b, the average maximum intensity of TCs is also projected to increase by 5 models, and decrease by 2 (HadGEM2-CC and HadGEM2-ES), but changes in intensity are small compared to changes in TC number (-1.5% to 4.8%).

3.4.3 Comments on method and results

The results obtained from this work using this method provide some initial indications of the response of CMIP5 models under scenarios of future climate change. However, these results should be viewed in the context of the following limitations. Firstly, the number of TCs detected in each model was found to be sensitive to the re-gridding method used, and the sensitivity of each model was noted to vary. Secondly, we note that the method used does not employ a 'warm core test on features identified for tracking, as several other tropical storm tracking methodologies do. These limitations mean that while the relative changes provide some useful indications of TC response under climate change scenarios, the absolute number of storms detected in each model should be interpreted with caution. Further investigation into the sensitivity of the results to these aspects of the methodology would provide useful contextual information to underpin any further applications of the results shown in this report.

Table A3.1 - A list of the CMIP5 models tracked, horizontal resolution of the models, number of baseline TCs identified and the threshold of 850hPa relative vorticity TCs had to satisfy to be counted. Those models in red are those which met the four criteria set out above.

Model	Resolution (no. of grid boxes)	No. of TCs 1971-2002	Relative vorticity threshold used for identification (x10-5 s-1)
bcc-csm-1-1-m	320x160	1680	5.5
bcc-csm-1-1	128x64	582	2.5
CanESM2	128x64	917	2.5
CMCC-CM	480x240	944	5.5
CNRM-CM5	256x128	913	3.0
CSIRO-Mk3-6-0	192x96	240	2.5
FGOALS-g2	128x60	707	3.0
FGOALS-s2	128x108	31	2.5
GFDL-CM3	144x90	19	2.5
GFDL-ESM2M	144x90	14	2.5
GFDL-ESM2G	144x90	14	2.5
HadGEM2-CC	192x144	607	4.5
HadGEM2-ES	192x144	671	4.5
inmcm4	180x120	63	2.5
IPSL-CM5A-LR	96x96	9	2.5
IPSL-CM5A-MR	144x143	77	2.5
IPSL-CM5B-LR	96x96	314	2.5
MIROC-ESM	128x64	89	2.5
MIROC-ESM-CHEM	128x64	96	2.5
MIROC5	256x128	896	3.0
MPI-ESM-LR	192x96	89	2.5
MPI-ESM-MR	192x96	63	2.5
MRI-CGCM3	320x160	1390	5.5
NorESM1-M	144x96	5	2.5

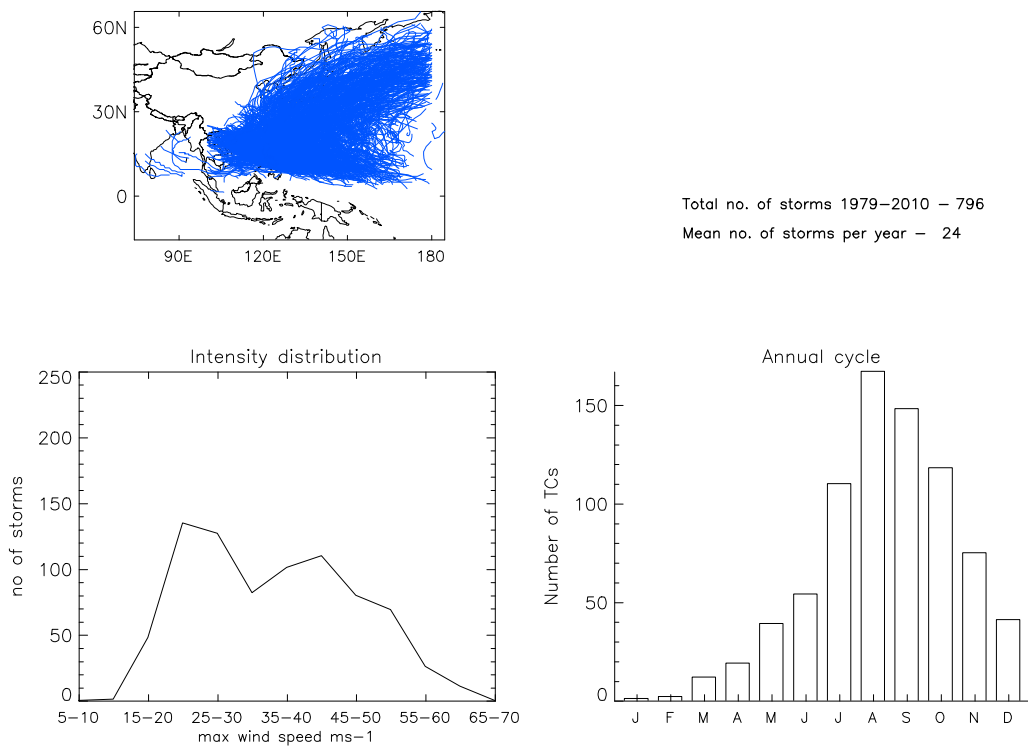


Figure A3.13, IBTrACS observations 1979-2010, TC tracks, number of TCs, Maximum 10m wind speed intensity distribution and annual cycle.

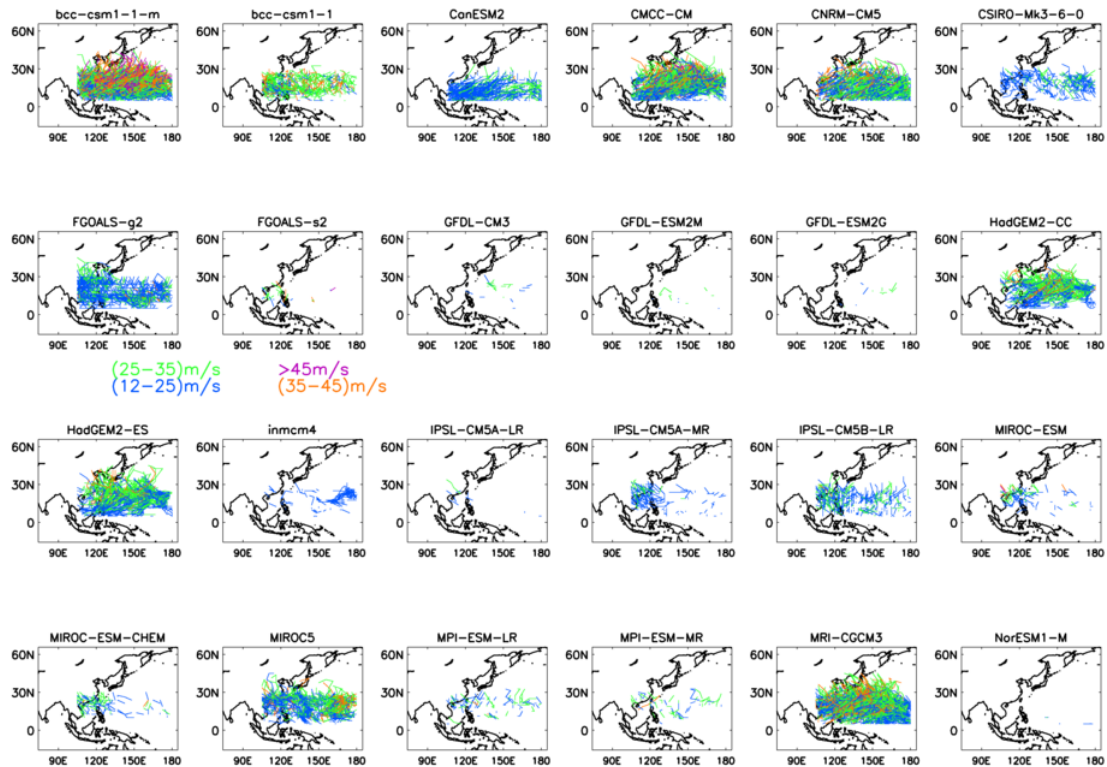


Figure A3.14, TC tracks in 24 members of the CMIP5 ensemble 1971-2020.

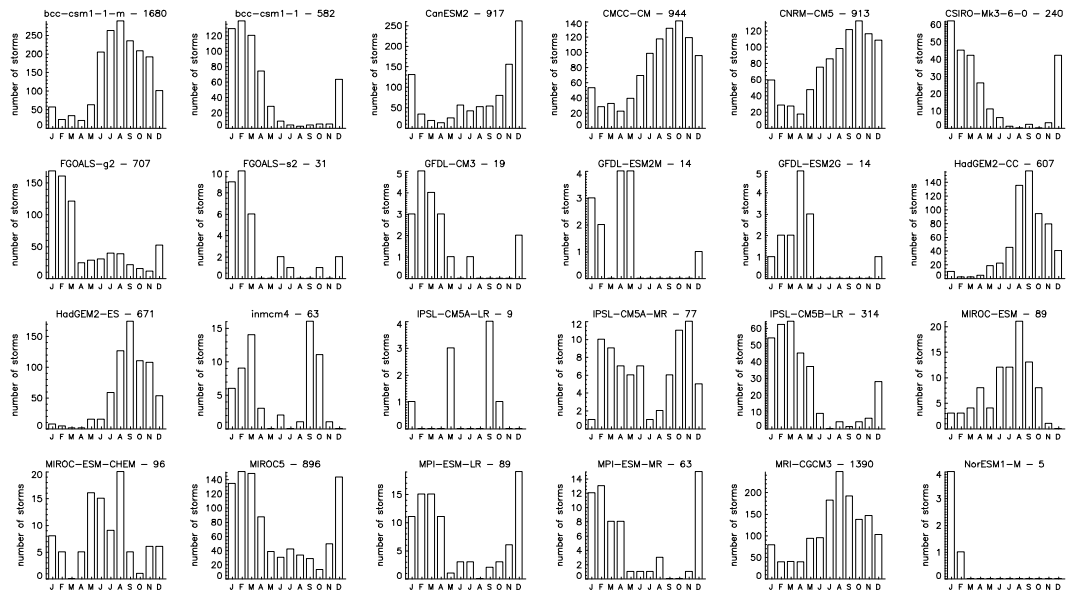


Figure A3.15, Annual cycle of North West Pacific TCs in 24 members of the CMIP5 ensemble 1971-2002. The total number of TCs is given next to the model name.

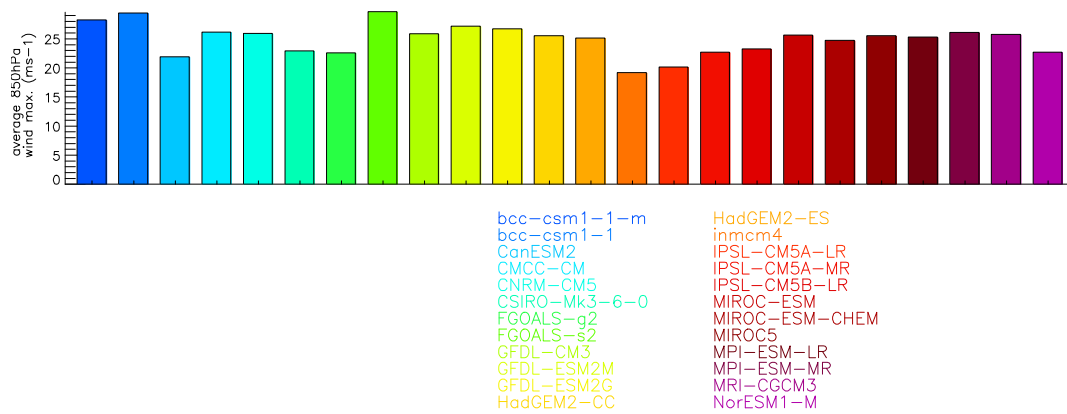


Figure A3.16, average maximum intensity of 850hPa wind speed (m/s) reached by TCs in 24 models of the CMIP5 ensemble.

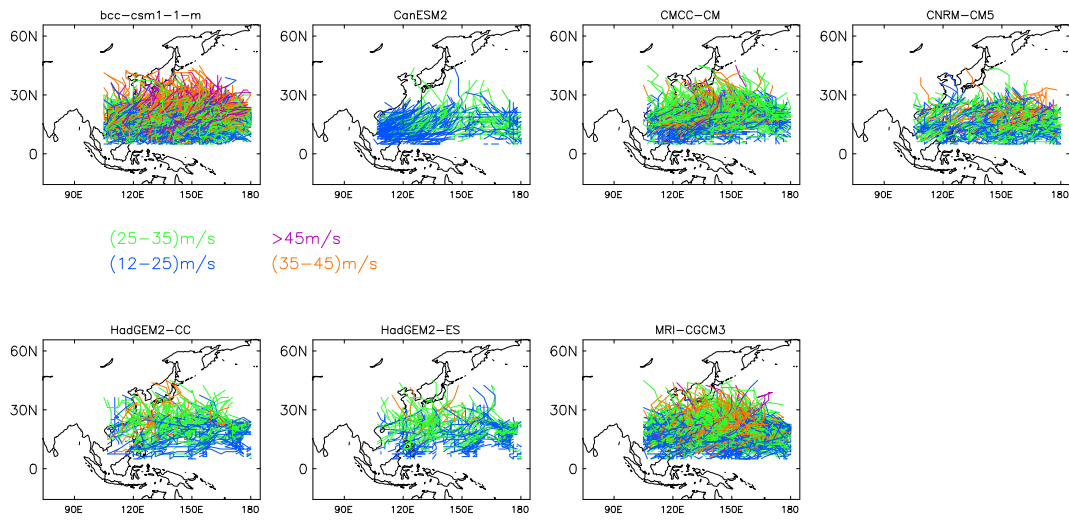


Figure A3.17, TC tracks (2064-2095) from CMIP5 models which meet the criteria set out in the method.

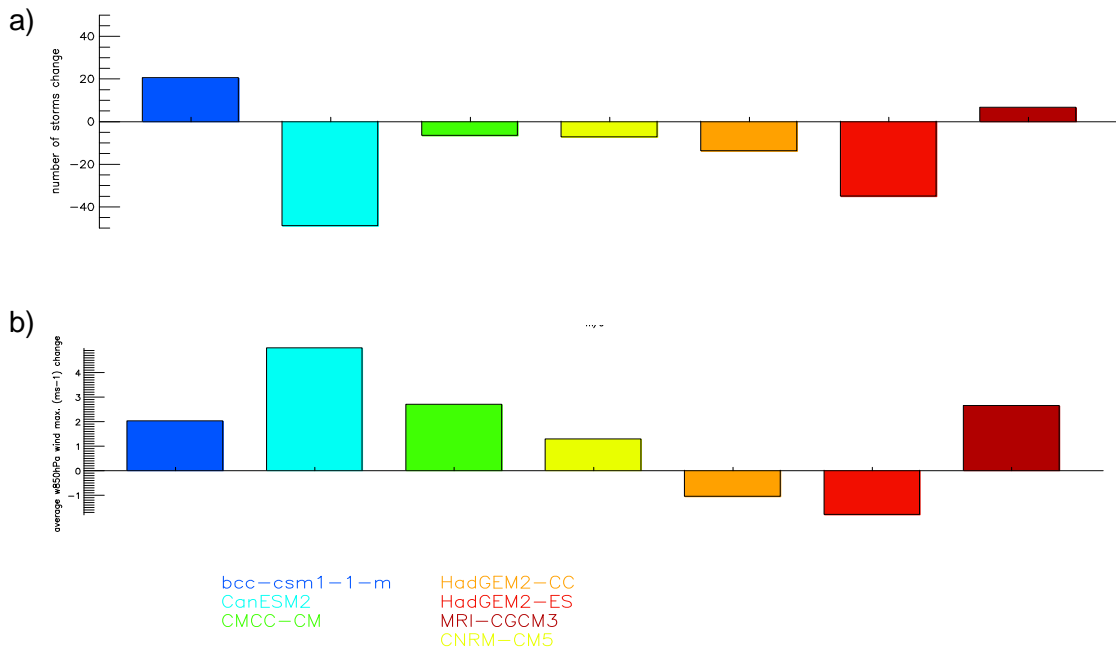


Figure A3.18, Percentage change in a) number of TCs and b) maximum 850hPa wind speed m/s 2064-2095 minus 1971-2002 from CMIP5 models which meet the criteria set out in the method.

Appendix 3.5: Description of sub-regions used to characterise the annual rainfall cycle

The broad region of south-east Asia contains a number of regions with different climate regimes. By using a number of smaller-sub-regions for assessing area-average climate, we can assess model performance in capturing the annual cycles within the region. Figure A3.19 shows the sub-regions used for the assessment of annual rainfall cycles in Southeast Asia.

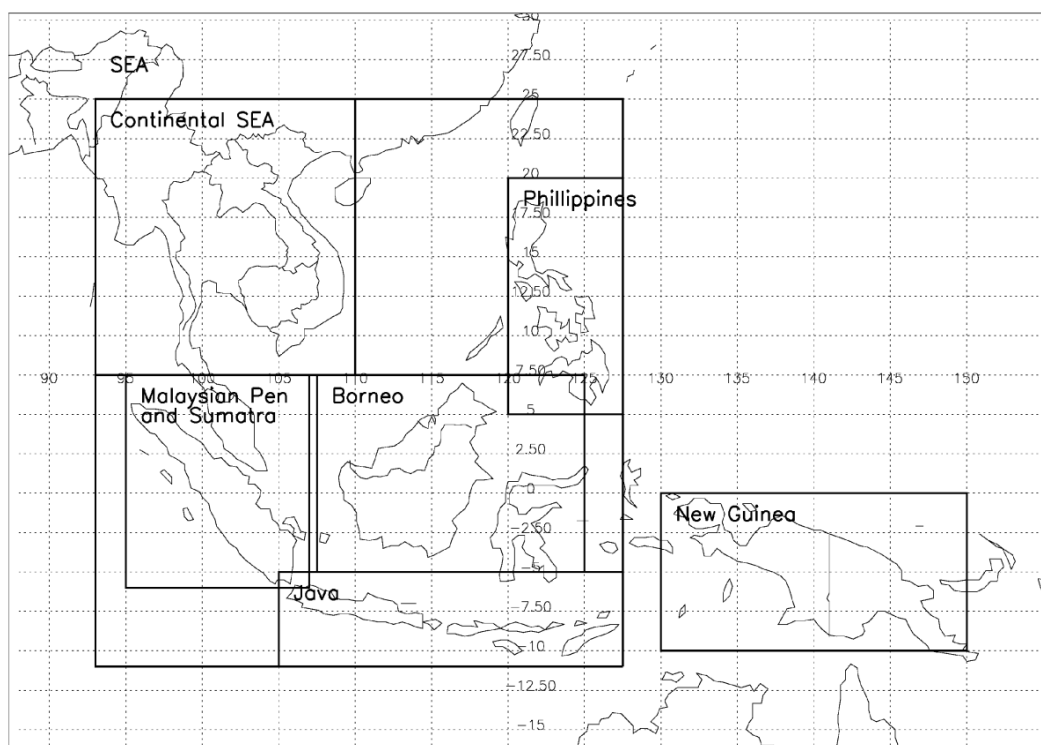


Figure A3.19: Regional definitions used to assess annual cycles of rainfall for key land regions of Southeast Asia.

Countries within Continental SEA experience a single rainy season during the southwest monsoon (May to October). The dry season lasts from November to April during the northeast monsoon when rainfall is light and infrequent. For coastal areas, the season of maximum rainfall is between September and January. During this period, these regions receive torrential rain from typhoons which move in from the South China Sea. There is a relatively large seasonal variation of temperatures over Continental SEA; the maximum temperatures usually reach near 40°C and temperatures may reduce to fairly low values, near or below 0°C in winter.

Most part of Philippines experience only a single season of heavy rain from July to October. Much of the rainfall comes from typhoons which produce very high wind speeds and torrential rain. These typhoons develop over the Pacific Ocean and move westward across the Philippines into the South China Sea. Coasts facing northeast are

exposed to the Pacific trade winds between November and March, and have their heaviest rainfall during this period. There is little seasonal variation in the mean annual temperature over Philippines.

The characteristic features of the climate over the southern part of Southeast Asia are uniform temperature, high humidity and copious rainfall. Generally, the climate can be divided into two main seasons, the Northeast Monsoon and the Southwest Monsoon season, which are separated by two relatively short inter-monsoon periods. There is no distinct wet or dry season, but rainfall is characterized by high intensities (measured in mm per hour) due to small to mesoscale convection cells of thunderstorms and squall lines.

Temperatures over southern Southeast Asia are generally uniform throughout the year because of the maritime characteristic of this region.

It has been shown in Cheong et al, (In review) the different impacts of ENSO and IOD on the precipitation and temperature over sub-regions similar to the ones used here. It was also stated in Yulihastin et al (Unpublished) that IOD has relatively stronger impact on western Indonesian climate and ENSO on the eastern Indonesian climate.

References

- Chang, C. P., P. A. Harr, and H. J. Chen, 2005: Synoptic disturbances over the equatorial South China Sea and western Maritime Continent during boreal winter. *Monthly Weather Review*, 133, 489-503.
- Chang, C.P., Z. Wang, J. McBride, C.H. Liu, 2005: Annual Cycle of Southeast Asia—Maritime Continent Rainfall and the Asymmetric Monsoon Transition. *Journal of Climate*, 18, 287–301.
- Cheong, W.K., N. Golding, S.Sirabaha, K.F. Kwan, T.A. Cinco, B. Archevarahuprok, V.H. Ho, D. Gunawan and S. Han (In review): Observed and Modelled Temperature and Precipitation Extremes over Southeast Asia from 1972-2010.
- Hu, Z. Z., R. G. Wu, J. L. Kinter, and S. Yang, 2005: Connection of summer rainfall variations in South and East Asia: Role of El Nino-southern oscillation. *International Journal of Climatology*, 25, 1279-1289.
- Hung, M., J. Lin, W. Wang, D. Kim, T. Shinoda, and S. Weaver, 2013: MJO and Convectively Coupled Equatorial Waves Simulated by CMIP5 Climate Models. *Journal of Climate*. doi:10.1175/JCLI-D-12-00541.1, in press.
- Lin, J. L., and Coauthors, 2006: Tropical intraseasonal variability in 14 IPCC AR4 climate models. Part I: Convective signals. *Journal of Climate*, 19, 2665-2690.
- Mitchell, T.D. and Jones, P.D., 2005: An improved method of constructing a database of monthly climate observations and associated high-resolution grids. *International Journal of Climatology* 25, 693-712

Tangang, F. T., L. Juneng, E. Salimun, K. M. Sei, L. J. Le, and H. Muhamad, 2012: Climate Change and Variability over Malaysia: Gaps in Science and Research Information. *Sains Malaysiana*, 41, 1355-1366.

Yulihastin, E., N. Febrianti, and T. Bannu: (Unpublished) Impacts of the ENSO and IOD on Indonesian Climate. National Institute of Aeronautics and Space (LAPAN), Indonesia.